Renewable and Sustainable Energy Reviews 82 (2018) 761–780

Contents lists available at ScienceDirect

Renewable and Sustainable Energy Reviews

journal homepage: www.elsevier.com/locate/rser

Advances in reforming and partial oxidation of hydrocarbons for hydrogen production and fuel cell applications

Sivaprakash Sengodan[a], Rong Lan[a], John Humphreys[a], Dongwei Du[a], Wei Xu[a], Huanting Wang[b], Shanwen Tao[a,b,*]

[a] School of Engineering, University of Warwick, Coventry CV4 7AL, UK
[b] Department of Chemical Engineering, Monash University, Clayton, Victoria 3800, Australia

ARTICLE INFO

Keywords:
Hydrogen production
Catalyst
Reforming
Partial oxidation
Fuel cells

ABSTRACT

One of the most attractive routes for the production of hydrogen or syngas for use in fuel cell applications is the reforming and partial oxidation of hydrocarbons. The use of hydrocarbons in high temperature fuel cells is achieved through either external or internal reforming. Reforming and partial oxidation catalysis to convert hydrocarbons to hydrogen rich syngas plays an important role in fuel processing technology. The current research in the area of reforming and partial oxidation of methane, methanol and ethanol includes catalysts for reforming and oxidation, methods of catalyst synthesis, and the effective utilization of fuel for both external and internal reforming processes. In this paper the recent progress in these areas of research is reviewed along with the reforming of liquid hydrocarbons, from this an overview of the current best performing catalysts for the reforming and partial oxidizing of hydrocarbons for hydrogen production is summarized.

1. Introduction

Fuel cells are electrochemical energy conversion devices that are used to convert the chemical energy stored in chemical fuels directly to electrical energy [1–5]. They offer many advantages such as high efficiency, low emissions, system compactness and environmental benefits when compared to conventional energy conversion technologies. Among the various types of fuel cells, solid oxide fuel cells (SOFCs) are well recognized due to advantages such as fuel flexibility, high tolerance to impurities in the fuel and not requiring expensive noble metal catalysts [6–14]. In conventional SOFCs, Ni-yttria stabilized zirconia (YSZ) is used as the anode and hydrogen is used as the fuel [15–17]. When this Ni-YSZ anode operated using hydrocarbon fuels instead of hydrogen then an efficiency increase can be seen at the system level [18–20]. However, when the Ni-YSZ anode is exposed to hydrocarbon fuels then carbon deposition will occur leading to the system failure [20–22]. When raw fuels, such as diesel, natural gas, and methanol are used, a fuel processor is needed to reform the hydrocarbons into a hydrogen rich gas for the fuel cell to perform the electrochemical conversion [23,24]. This has led to a great interest in converting hydrocarbons into hydrogen. Fuel processing technologies for high temperature fuel cells involve the conversion of hydrogen rich fuels such as gaseous hydrocarbons, gasoline, ammonia, or methanol into a hydrogen rich stream [25,26].

The development of converting hydrocarbon fuels to hydrogen-rich gas products generally fall in one of following processes: steam reforming (SR), auto thermal reforming (ATR), dry reforming (DR), partial oxidation (POX) or a combination of two or more [27]. In spite of their advantages, each of these processes is limited due to factors such as design, fuel and operating temperature. A range of fuel cell systems and common fuel reforming methods have been reviewed by Larminie and Dicks [28]. Thermodynamical analyses of the reforming processes for producing fuel cell feeds of the necessary quality using different fuels have been carried out. In 2006, reforming catalysts for hydrogen generation in fuel cell applications was reviewed by Cheekatamarla et al. [27] There is currently a wide selection of potential fuel reforming catalysts receiving research attention. When investigating a fuel reforming catalyst for fuel cell applications the critical consideration are weight, size, activity, cost, transient operations, versatility to reform different fuels/compositions, catalyst durability and fuel processor efficiency. A suitable catalyst for fuel reforming will catalyze the reaction at low temperatures, is resistant to coke formation, and is tolerant of different concentrations of poisons (e.g. sulphur, halogens, heavy metals, etc.) for an extended period of time. The challenges and opportunities of various fuel reforming technologies for applications in low and high-temperature fuel cells have been previously reviewed [27,29–31]. In previous papers the various steps involved in the generation of fuel cell grade hydrogen with respect to catalyst development

* Corresponding author at: School of Engineering, University of Warwick, Coventry CV4 7AL, UK.
E-mail address: S.Tao.1@warwick.ac.uk (S. Tao).

http://dx.doi.org/10.1016/j.rser.2017.09.071
Received 28 July 2016; Received in revised form 3 July 2017; Accepted 19 September 2017

has been discussed [32–35]. A couple of excellent reviews on CO_2 reforming and partial oxidation of methane are also available [36,37]. The production of hydrogen from steam reforming of ethanol and glycerol was also reviewed in 2005 and 2009 respectively [38,39]. The goal of the present paper is to review and discuss recent progress in the catalyst development, particularly, steam reforming and partial oxidation catalysts and their ability to generate hydrogen from different fuel sources for fuel cell applications. The focus will be on transition metals supported on mixed metal oxides and perovskites oxides. This paper surveys four key processes in H_2 and syngas production technologies in the following sections, including Section 2 internal reforming for hydrogen production in solid oxide fiuel cells, Section 3 – external reforming for hydrogen production (steam reforming of methane, partial oxidation of methane, CO_2 Reforming of methane) Section 4 – reforming of liquid hydrocarbons, Section 5 poisoning of catalyst and in Section 6 – reforming and partial oxidation catalysts for direct hydrocarbon solid oxide fuel cells. A summary section is also provided with descriptions on challenges and future work (Section 7), followed by the conclusion section. Some key papers in previous studies are also cited.

2. Internal reforming for hydrogen production

Among the various types of fuel cell systems, SOFCs can offer more fuel flexibility by internal reforming of hydrocarbon fuels such as methane, propane, ethanol and natural gas, at the anode [40–42]. Among the various hydrocarbon fuels, methane and propane are the most widely available with vast supply worldwide. By internally reforming hydrocarbon fuels in the SOFCs then an increase in efficiency can be observed as well as simplifying the integration of the system. For example, Eric et al. [43], reported that the efficiency of the internal reforming is 8% higher, compared to the external reforming in the same SOFC system. Simplified thermal management and higher fuel cell performance can be achieved when internally reforming of the fuel is used over external reforming. Also, the internal reforming process in SOFCs can be operated at low steam/carbon ratios compared to the external reforming process. When carrying out internal reforming in a SOFC, it should be noted that the conventional Ni based anode cermet will display poor catalytic activity towards the hydrocarbon and steam/CO_2 reforming due to carbon deposition at the Ni cermet anode. The catalytic modification of conventional Ni cermet anode for direct internal reforming is more useful than the identification of new anodes which are tolerant to hydrocarbon fuels. In order to improve the reforming reaction of the hydrocarbons while also improving the stability of the Ni cermet anode against carbon deposition a layer of reforming catalyst can be deposited over the Ni anode. Under the direct internal reforming conditions, hydrocarbon fuels with steam/CO_2 are passed through the catalytic functional layer, where the fuel is converted into syngas before it reaches the anode. The catalytic layer requires particular properties such as a high catalytic activity towards hydrocarbon reforming and high resistance against carbon deposition. Thus the greater partial reforming reactions occur at the functional catalyst layer with the hydrocarbon fuels converted into syngas as they reach the cermet anode.

Zhan et al. [19] first demonstrated the use of Ru-CeO_2 catalyst as a direct internal reforming catalyst with the Ni cermet anode. They applied a porous Ru-CeO_2 catalyst layer against the Ni cermet anode side of the fuel cell. This porous Ru-CeO_2 catalyst layer is used to internally reform the hydrocarbons into syn-gas. Sun et al. studied the effect of morphological features of CeO_2 catalyst on direct internal reforming the hydrocarbons [44]. The performance of the fuel cell with mesoporous flower like Ru-CeO_2 catalyst shows a power density up to 654 mW cm^{-2} at 600 °C [45]. Klein et al. studied the Ir (0.1 wt%)-CeO_2 catalyst on Ni-YSZ cermet anode in CH_4 fuel [46,47]. Fig. 1 shows the anodic gas phase composition compared to current of the cell in pure methane fuel at 900 °C. H_2 and CO are the only major products for the internal reforming reaction occurring at the catalyst layer. Fuel cells

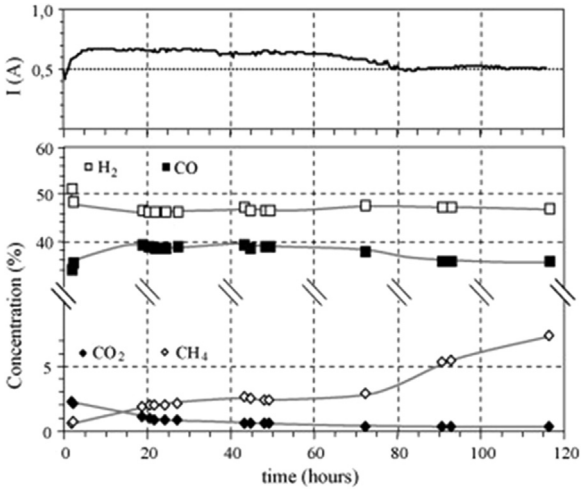

Fig. 1. Evolution as a function of time of the anodic gas phase composition compared to the current of the cell; the cell was operated at V = 0.6 V in pure CH_4 with a total flow rate of 4 sccm; dashed line represents the levels measured at OCV in diluted H_2 at 900 °C [46].

with an Ir-CeO_2 catalyst show stable fuel cell operation for 120 h in methane at 900 °C and 0.6 V yields a current density of about 100 mA cm^{-2} [46]. However, it has been noted that the methane concentration gradually increased after 70 h (Fig. 1) indicating that the reforming or partial oxidation activity of the anode started to decrease at this time, however, the fuel cell performance was not affected. One of the possible reasons for this may be due to other mechanisms, such as the direct oxidation of methane playing an important role in retaining the stable current.

Wang et al. [48] studied the effect of Ru loading and their catalytic activities on Al_2O_3 supported catalysts for internal reforming of methane by partial oxidation, steam reforming and CO_2 reforming under SOFC operating conditions. They found that 1 wt% Ru-Al_2O_3 catalyst shows insufficient catalytic activity towards methane reforming. A 3 wt% Ru-Al_2O_3 catalyst shows an outstanding stability and a good thermal stability with the Ni-YSZ anode. Fig. 2 shows the electrochemical performance of 3 wt% Ru-Al_2O_3 anode in H_2, methane-oxygen, methane-steam and methane-CO_2 gas mixtures. At 850 °C, the fuel cell using a methane-oxygen mixture shows a peak power density of 1006 mW cm^{-2}, while the same fuel cell shows 1038 mW cm^{-2} in pure H_2.

It has been found that addition of metal oxides can improve coke resistance property. Wang et al. [49–51] also studied the effect of promoters Li_2O, La_2O_3, CaO, CeO_2, Pr_2O_3, Sm_2O_3 and Gd_2O_3 on the Ni-Al_2O_3 catalyst with the aim of improving its coking resistance during fuel cell operation with methane fuels. Among the various promoters, LiLaNi/Al_2O_3 showed the best catalytic activity and stability compared to LaNi-Al_2O_3 and LiNi-Al_2O_3 catalysts. Lee et al. [52] studied the effect of pore formers in the Ni-Fe anode reforming catalyst on Ni-YSZ fuel cell. The fuel cells containing pore formers (10 wt% carbon black (HB170)) in the Ni-Fe catalyst layer exhibited the highest power density, when compared to the fuel cell containing Ni-Fe catalyst layer without pore formers. It should be noted that some oxides such as CaO, Li_2O may react with CO_2 to form stable carbonate thereby losing their promoting effects. Liao et al. [53], studied the doped ceria $Ce_{0.8}Zr_{0.2}O_2$ catalyst for direct internal reforming of ethanol. The high oxygen storage capacity, thermal stability and the ability of doped ceria to promote the water gas shift reaction makes $Ce_{0.8}Zr_{0.2}O_2$ a good catalyst for internal reforming. The catalytic activity is also related to the synthesis process. Liao et al. used different synthesis processes to prepare the Ni-$Ce_{0.8}Zr_{0.2}O_2$ catalyst. Ni- $Ce_{0.8}Zr_{0.2}O_2$ catalyst prepared by the glycine nitrate process (GNP) exhibited the best catalytic properties compared to the Ni- $Ce_{0.8}Zr_{0.2}O_2$ catalyst prepared by the infiltration method. Above 600 °C, both the Ni- $Ce_{0.8}Zr_{0.2}O_2$ catalysts show a high and

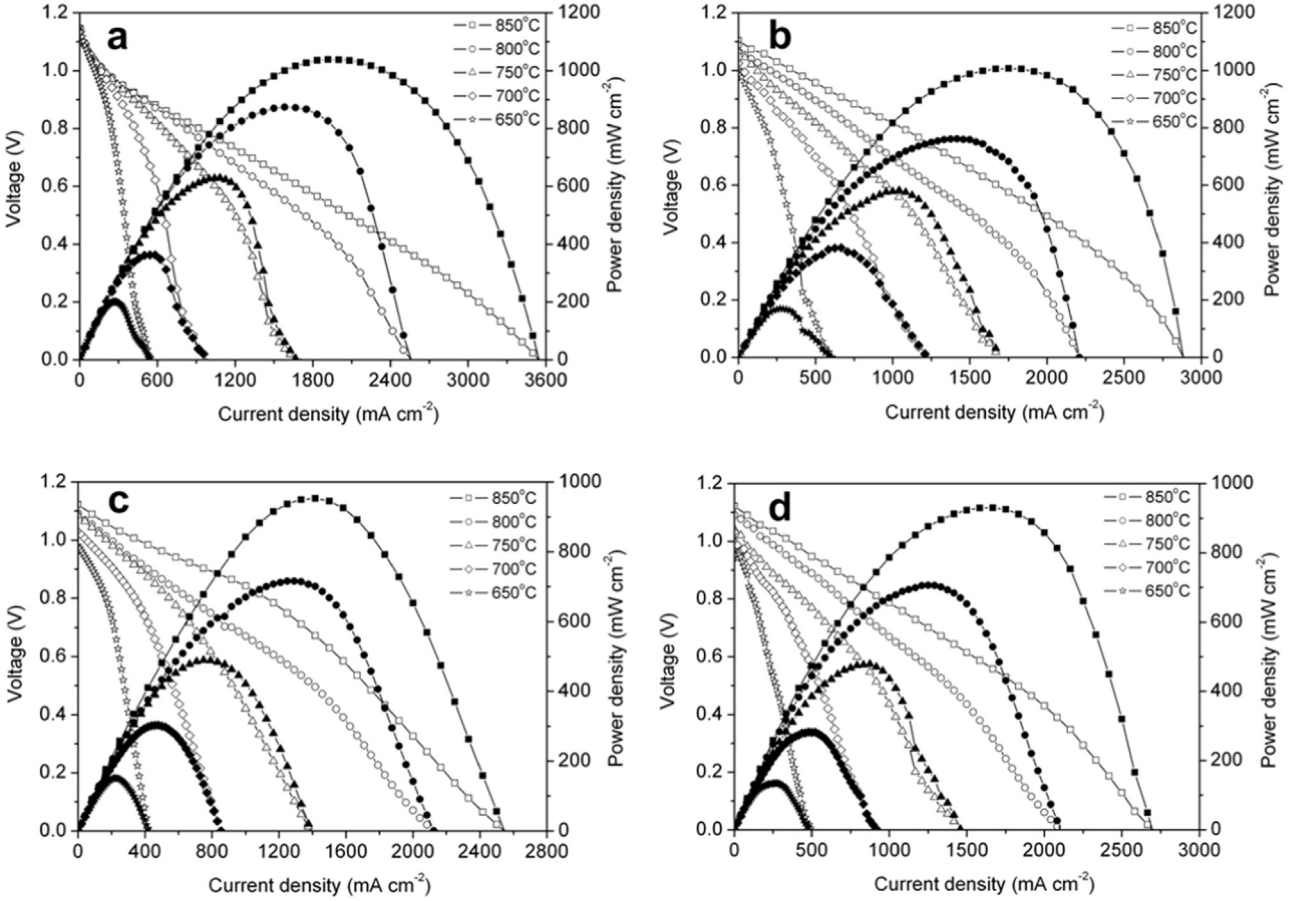

Fig. 2. *I-V* and *I-P* curves of the fuel cells with the 3 wt% Ru-Al_2O_3 catalyst layer operating on a mixed gas composed of pure hydrogen (a), 80% CH_4 and 20% O_2 (b), 66.7% CH_4 and 33.3% H_2O (c) and 66.7% CH_4 and 33.3% CO_2 (d) at different temperatures [48].

comparable selectivity for H_2. However, the catalytic activity decreases significantly at low operation temperatures. At 400 °C, the Ni-$Ce_{0.8}Zr_{0.2}O_2$ catalyst prepared by the GNP method shows 70% H_2 selectivity, while the infiltrated catalyst shows 60.2% selectivity. Ye et al. [54] also studied the ethanol steam reforming over Cu-CeO_2 catalyst. Fuel cells prepared with 21.5 wt% Cu-8.5 wt% CeO_2- scandia stabilized zirconia (ScSZ) show power densities of 372 mW cm^{-2} at 800 °C when C_2H_5OH + H_2O (2:1) was used as the fuel.

In addition to stabilized zirconia based and doped cerium oxide based fuel cells, some proton conducting oxides have also been investigated as materials for internal reforming in fuel cells [55,56]. Azimova et al. [55] studied the $BaCe_{0.48}Zr_{0.4}Yb_{0.1}Co_{0.02}O_3$ perovskite type proton conducting oxides for direct internal reforming of methanol. Fig. 3 shows the electrochemical performance of a methanol/steam fueled proton conducting SOFC at 600 °C. The fuel cell shows a maximum power density of 65 mW cm^{-2} in 3:1 (S:C) methanol/water fuel.

Jin et al. [57,58], has reported the use of $Cu_{1.3}Mn_{1.7}O_4$ spinel type oxide internal reforming catalyst layer for methane fueled Ni – $Sm_{0.2}Ce_{0.8}O_{1.9}$ (SDC) SOFC. The fuel cells using the $Cu_{1.3}Mn_{1.7}O_4$ anode catalyst have been shown to exhibit similar electrochemical activities comparable to that of the Ni–SDC anode without a catalyst layer. However, the fuel cells composed of a $Cu_{1.3}Mn_{1.7}O_4$ anode catalyst layer shows a stable performance after 60 h in methane, while the fuel cell without the catalyst layer deactivated quickly in methane.

It was found that addition of BaO onto the Ni-based anode can improve the anti-coking property [59]. It was found that nanosized BaO islands grow on the Ni surface, creating numerous nanostructured BaO/Ni interfaces that readily adsorb water and facilitate water-mediated

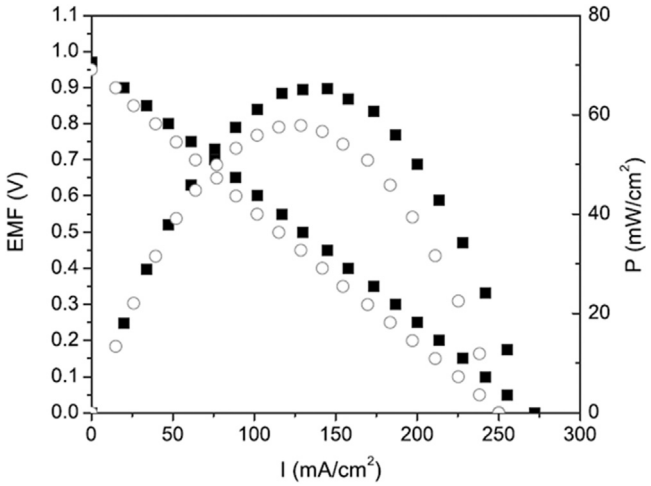

Fig. 3. *I-V* and *I-P* curves of the Ni- $BaCe_{0.48}Zr_{0.4}Yb_{0.1}Co_{0.02}O_3$ fuel cell anode in 2:1 S:C methanol/water (○) and 3:1 S:C methanol/water (■) fuels at 600 °C [55].

carbon removal reactions. Besides the metal – metal oxide cermets, some redox stable oxide anode are also used as anode for SOFCs [4,60,61]. At the anode, internal reforming is possible with the presence of H_2O and CO_2 when hydrocarbon fuels are used in SOFCs. The catalytic activity of these redox stable oxides is very much related to their composition. For example, $La_{0.75}Sr_{0.25}Cr_{0.5}Mn_{0.5}O_{3-\delta}$ (LSCM) is a good methane oxidation catalyst while $La_{0.75}Sr_{0.25}Cr_{0.5}Fe_{0.5}O_{3-\delta}$ (LSCrF) is an excellent reforming catalyst [10,11]. The use of some

oxides can prevent the coking on the anode when hydrocarbon fuels are used in SOFCs [60,61].

3. External reforming for hydrogen production

The production of hydrogen rich fuels from hydrocarbons can be achieved through either internal or external steam reforming; from this well established process high efficiency for hydrogen production can be achieved. However, the overall steam reforming reaction is endothermic and is generally carried out at the fuel cells high operating temperatures, typically between 500 to 800°C in the presence of a suitable catalyst. The steam reforming reaction can be generalized as follows for hydrocarbon fuels,

$$C_nH_m + nH_2O \rightarrow nCO + (n + 1/2m)H_2 \quad (1)$$

3.1. Steam reforming of methane

Steam reforming catalysts must meet stringent requirements such as high activity on hydrocarbon conversion, high activity stability, good heat transfer, low pressure drop, high selectivity to hydrogen, high thermal stability and excellent mechanical strength [24]. Steam reforming of methane is a popular method for syngas production and a number of catalysts containing both noble metals and transition metals have been investigated. Catalysts based on Ni have been found to have high catalytic activity and high selectivity for steam reforming of methane (SRM). However, Ni based catalysts also have high carbon coking during SRM. The coking resistance of the Ni catalyst can be improved by the addition of small amounts of noble metals, rare earth metals and supporting materials like perovskites. Since the effects of the additives and support material for the Ni-based catalyst can drastically improve both catalytic performance as well as stability, research in to these areas is very important. The support and additive can be directly involved in the reaction steps facilitating the absorption of the reactant and product formation. Table 1 summarizes the chemical composition of Ni-metal/support catalysts and noble metal/support for steam reforming of methane. Some recently reported examples are briefly discussed. The SRM involves two endothermic reactions (steam reforming) and the exothermic reaction (water gas shift reaction) as follows:

$$CH_4 + H_2O \leftrightarrow CO+3H_2 \quad \Delta H^{\circ}_{298\,K} = 206.1 \text{ kJ mol}^{-1} \quad (2)$$

$$CO + H_2O \leftrightarrow CO_2 + H_2 \quad \Delta H^{\circ}_{298\,K} = -41.1 \text{ kJ mol}^{-1} \quad (3)$$

$$CH_4+2H_2O \leftrightarrow CO_2+4H_2 \quad \Delta H^{\circ}_{298\,K} = 165.1 \text{ kJ mol}^{-1} \quad (4)$$

When Ni-metal/support is used as the SRM catalyst, we have to pay close attention to preparation methods in order to ensure that a high catalytic activity is achieved for the modified catalysts. A typical catalyst synthesis method is the impregnation method using an aqueous solution containing Ni. When Ni/SiO_2 catalyst was prepared by impregnation method followed by dielectric barrier discharge (DBD) it shows an advantage of having smaller particle sizes, leading to a moderate methane decomposition rate and a better balance between carbon depositions. Besides, the catalyst prepared conventionally by calcination shows a much larger particle size [62].

In a recent work, Zhang et al. [62] studied SRM over Ni based core shell catalyst Ni/Al_2O_3 – silicalite zeolite by different synthesis methods. The catalyst consists of a Ni/Al_2O_3 core and silicalite zeolite shell. Their main finding shows that an inactive $NiAl_2O_4$ spinel phase was formed during repeated calcination at elevated temperatures. Among the catalysts tested the catalytic activity of the core shell catalyst for the SRM reaction displayed a 10% improvement over catalysts prepared by traditional method.

Cerium oxide was used as a support material for nickel catalysts and the effect of SRM at a temperature of 800 °C was investigated by Wang et al. [63]. A template synthesis process has been adopted to prepare hierarchically structured NiO/CeO_2 nanocatalysts. The template catalyst is fabricated by interwoven ceramic fibers, and the fibers have a nanoporous structure with NiO nanoparticles supported on a CeO_2 scaffold. Catalyst calcination temperature and its microstructure have a strong influence on SRM. The catalyst calcined at 950 °C shows the highest performance and stable methane conversion due to its optimized microstructure. Methane conversion was reported about 98% at 800 °C and a steam/CH_4 ratio of 2. No catalyst decay was found within 300 min due to the hierarchical microstructure of the nanocatalyst.

A number of catalysts based on noble metals such as Ru, Pt, Pd, Ir etc. were tested under methane steam reforming conditions with various supports. Among them, Pd-Rh metal foam (Pd 1.5 wt%, Rh 0.16 wt %, ZrO_2 35 wt%, Al_2O_3 63.7 wt%) has been shown to exhibit good activity and stability in the hydrothermal SRM environment compared to commercial $Ru/\gamma\text{-}Al_2O_3$ and Ni/Al_2O_3 catalysts [90]. At 800 °C the Pd-Rh/metal foam catalyst exhibited steady activity with negligible coke deposition after a stability test of 200 h.

For SRM, Ru catalysts have been shown to be very active and selective for H_2 production. Simakov et al. [89], reported that $Ru/\gamma\text{-}Al_2O_3$ catalysts with different Ru loadings of 0.07, 0.15, 0.30, 1 and 3 wt% can be synthesized by sonication-assisted wet impregnation using ruthenium(III) chloride as a precursor, high surface area aluminum oxide as a support, and acetone as an impregnation medium. $Ru/\gamma\text{-}Al_2O_3$ (0.15 wt % loading) catalyst outperforms the commercial (12 wt% $Ni\text{-}Al_2O_3$) catalyst by two orders of magnitude in terms of methane conversion normalized by metal loading. The minimum limit of the Ru loading is 0.15 wt%, if this limit is lowered; the Ru catalyst activity declines significantly which was attributed to the oxidation of sub-nanometer Ru clusters [89]. However, another possibility is that the active site is insufficient to achieve high activity when loading is too low. It was reported that the commercial $Ni/\alpha\text{-}Al_2O_3$ catalyst was relatively stable at steam to carbon ratio (S/C) = 3 but deactivated rapidly at S/C = 2, losing ca. 70% activity over the course of 15 h [89] while the $Ru/\gamma\text{-}Al_2O_3$ catalysts is stable even at a low steam to carbon ratio of 1. As shown in Table 1, it is generally difficult to achieve high conversion at a low steam to carbon ratio.

The effect of Pd catalysts supported on alumina and mixed with $La_2O_3\text{-}Al_2O_3$ oxides was studied by Cassinelli et al. [91]. The authors found that the catalytic performances of Pd catalysts in SRM were significantly affected by the type of support. La-containing Pd catalysts exhibit specific reaction rates in the SRM reaction at 490 °C compared to Pd supported on Al_2O_3, this is due to the different electronic state of Pd. The formation of $Pd^{\circ}[Pd^{\delta+}O_xLa]$ species with La support was found to promote the CH_4 activation and carbon oxidation. Their results show that the nature of support and the metal–support interface play a very significant part in the design of highly active and stable Pd catalysts in SRM.

The effect of support material on the surface and catalytic properties of the Pt catalyst when used for SRM were investigated by Rocha et al. [92]. The $Pt/La_2O_3\text{-}Al_2O_3$ and Pt/Al_2O_3 catalyst was obtained by impregnation of the support with an ethanolic solution of $H_2PtCl_6{\cdot}6H_2O$. Through extended X-ray absorption fine structure (EXAFS) results it has been shown that the Pt nanoparticles are anchored by weak interaction with the support, the higher stability of Pt catalyst obtained when the $La_2O_3\text{-}Al_2O_3$ support was used instead of the Al_2O_3 is related to the higher thermal stability of Al_2O_3 modified with lanthanum. The catalytic activity of Pt supported catalysts for SRM depends on the availability of CH_4 to Pt active sites.

Yu et al. have prepared Ag-Ni alloy catalysts supported on CeO_2 for the reforming reaction of methane and carbon dioxide through the impregnation method [93]. The samples have different Ag content with 10 mol% Ni as active sites and 0.3 mol%, 0.6 mol% and 2.4 mol% Ag as the promoter. Table 2 shows the assignments of the fitting components for C1s, Ag 3d, Ni2p3/2 and Ce 3d in X-ray photoelectron spectroscopy (XPS) spectra for Ag promoted Ni/CeO_2 catalyst to determine the chemical states and surface compositions. The Ni content at the surface

Table 1
Chemical composition of Ni-metal/support catalyst and noble metal/support for steam reforming of methane.

Catalyst	Preparation method	Temperature (°C)	Weight hour space velocity (ml h^{-1} g_{cat}^{-1})	Steam to carbon ratio (S/C)	Conversion (%)	H_2 selectivity (%)	Ref.
$Ni/La_2Zr_2O_7$	Coprecipitation/ impregnation	800	18,000	2	100	> 75	[64]
Ni-nano-CaO/Al_2O_3	impregnation	600	2700	4	86	92	[65]
Ni/γ-Al_2O_3	impregnation	655	n/a	3	88		[66]
Ni–Pt/ Al_2O_3 anodic alumina support	impregnation	700	471,000	3	100	75	[67]
Ni/SiO_2	impregnation	800	24,000	0.5	40	NA	[62]
Pt-Ni/Al_2O_3	impregnation	650	96,000	1	77.2	68.3	[68]
Ni-$Pt/MgAl_2O_4$	impregnation	600	9600	4	80	NA	[69]
Ni-Cu/Al_2O_3	impregnation	500	2000	3	> 85	> 97	[70]
Ni-Rh/Al_2O_3	impregnation	800	6000	3	32.2	NA	[71]
Ni-Au/Al_2O_3	impregnation	550	3000	4	84	NA	[72]
$Mo/Ni/Al_2O_3$	Precipitation/ impregnation	700	24,000	4	85	55	[73]
Ag-Ni/Al_2O_3	impregnation	600	105,000	0.5	> 30	NA	[74]
$Ni@SiO_2$	Stöber process/ deposition precipitation	750	6600	3	85	45	[75]
$Ni/MgSiO_3$	impregnation	650	42,000	2.5	82	NA	[76]
$M/Ni_{0.5}/Mg_{2.5}$(Al)O M = Rh, Pt, Pd	co-precipitation	700	210,000	2	> 85	NA	[77]
$M/Ce_{0.15}Zr_{0.85}O_2$ M = Pt, Ru, Rh	urea hydrolysis/ impregnation	800	54,000,000	2	98.6	NA	[78]
$Ni/Ce_{1-x}Gd_xO_2$	hydrolysis	700	560,000	3	75	NA	[79]
Ni/ CeO_2-HfO_2	EDTA-citrate method/ impregnation	700	25,500	2	85	NA	[80]
Ni/CaO–ZrO_2-Al_2O_3		600	60,000	1	45	35	[81]
$Ru/Ni_xMg_{6-x}Al_2$	Hydrotalcite process/ impregnation	800	30,000	1	85	NA	[82]
$Ru/Co_{6-x}Mg_xAl_2$	hydrotalcite route/ impregnation	600	15,000	3	80	NA	[83]
Ru/MgO-Nb_2O_5	impregnation	700	20,000	4	> 95	> 72 NA	[84]
Rh/CeO_2	impregnation	800	40,000	1.2	99.4	NA NA	[85]
Rh/xSm_2O_3-$yCeO_2$.Al_2O_3	sol–gel/ impregnation	760	6,480,000	3	70	NA	[86]
$Zr_{0.95}Ru_{0.05}O_{2-\delta}$	sonochemical method	650	61,800	1	74	81	[87]
$LaNiO_3$	spray pyrolysis	777	300,000	1	75	NA	[88]
Ru/γ-Al_2O_3	sonication-assisted wet impregnation	600	750	1	75	68	[89]

of Ni/CeO_2 is estimated to be higher than that in the bulk, indicating a surface enrichment of Ni on the Ni/CeO_2. For 0.3 mol% Ag Ni/CeO_2 and 2.4 mol% Ag Ni/CeO_2, the surface contents for Ni are still higher than that of the bulk surface, showing Ag does not affect the Ni content enrichment at the catalyst surface. Generally, as Ag and Ni form surface alloys on the Ni surface, the Ag content should be higher than that in the bulk in the XPS measurement. The difference came from fact that partially reduced CeO_2 can migrate onto the Ni surface and bury Ni particles into the catalyst support. The CeO_2 migration causes the Ni enrichment at the Ag-Ni/CeO_2 surface. The catalyst with 0.3 mol% Ag loading subjected to a stability test was shown to be resistant to coke deposition. 0.3 mol% Ag decreases the intrinsic activity of Ni surfaces and concurrently increases the long term (100 h) stability under various feedstock conditions. Also, the Ag promoter decreases the coke formation and modifies the coke from whisker carbon or graphitic carbon to amorphous carbon.

SRM on the Sn/Ni/YSZ catalyst was reported by Nikolla et al. through a combination of kinetic studies, isotopic-labeling experiments, and DFT calculations [94–96]. Fig. 4 shows the kinetic isotope studies on Ni/YSZ and Sn/Ni/YSZ catalyst surface with labeled methane CD_4 [95]. They reported that kinetic isotope effects are similar in degree by the rate of C–H bond dissociation on both catalysts. From this kinetic we are able to draw conclusions about the mechanisms accountable for the improved carbon-tolerance of Sn/Ni compared to Ni. Sn atoms are reasonable for the rate-controlling CH_4 activation step to move from low-coordinated Ni sites to the well-coordinated Ni-Sn sites. Sn preferentially displaces the Ni atoms from the under-coordinated sites. In presence of the Sn, the activation barrier for the dissociation of CH_4 is

Table 2
Assignments of the fitting components for C1s, Ag 3d, Ni2p3/2 and Ce 3d in XPS spectra of catalyst [93].

Catalysts	C 1s	Content (at%)	Ag 3d	Content (at%)	Ni 2p3/2	Content (at%)	Ce 3d	Content
Ni/CeO_2	Ni_3C	0.00%			Ni°	27.26%	Ce^{4+}	83.45%
	Graphite	83.03%			Ni^{2+}	72.74%	Ce^{3+}	16.55%
	CO_3^{2-}	16.97%						
Ni/CeO_2–0.3Ag	Ni_3C	0.63%	Ag	74.05%	Ni°	21.98%	Ce^{4+}	74.35%
	Graphite	90.81%	Ag_n^+	25.95%	Ni^{2+}	78.02%	Ce^{3+}	25.65%
	CO_3^{2-}	8.56%						
Ni/CeO_2–2.4Ag	Ni_3C	7.93%	Ag	86.63%	Ni°	6.40%	Ce^{4+}	59.44%
	Graphite	65.89%	Ag_n^+	13.37%	Ni^{2+}	93.60%	Ce^{3+}	40.56%
	CO_3^{2-}	26.17%						

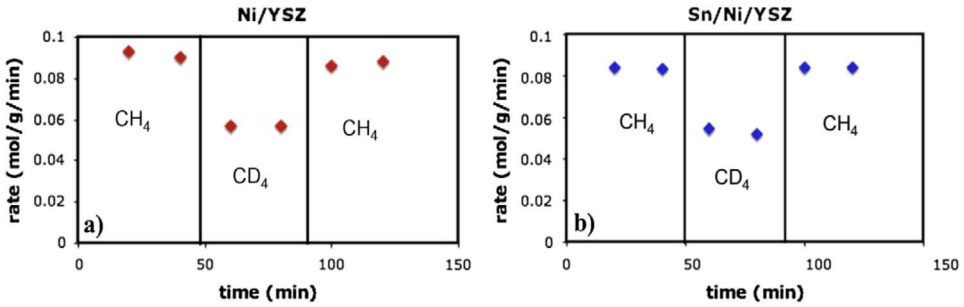

Fig. 4. The rate of steam reforming is measured for CH_4 and CD_4 reactants as a function of time on (a) Ni/YSZ at 700 °C and (b) Sn/Ni/YSZ at 760 °C. The dark lines depict points in time when the reactant is switched from CH_4 to CD_4 and back to CH_4. The steam-to-carbon ratio was 1 [95].

increased while also decreasing the binding of the carbon atoms to the low-coordinated sites. This will thereby inhibit the nucleation of carbon at Ni sites. In other words, the Sn alloying with Ni atoms preferentially oxidize C atoms from C–C bonds and/or decreasing the thermodynamic driving force for carbon nucleation on Ni sites.

A Cu promoted Ni/Al_2O_3 was prepared and studied by Khzouz et al. [70] in order to improve the SRM and suppress the carbon deposition. The activity of $Cu\text{-}Ni/Al_2O_3$ was compared with that of commercial Ni/Al_2O_3, $Cu/ZnO/Al_2O_3$ catalysts. Morphological characterization results showed that the average particle size increases when compared to the commercial Ni/Al_2O_3 catalyst. The prepared $Cu\text{-}Ni/Al_2O_3$ catalyst exhibited low selectivity for CO and it was shown to be more selective to H_2 in methane. Fig. 5 shows the SRM for $Cu\text{-}Ni/Al_2O_3$ and the commercial Ni/Al_2O_3 catalyst. The $Cu\text{-}Ni/Al_2O_3$ catalyst showed a methane fuel conversion of 98% with 99% hydrogen selectivity at 650 °C. The improved performance of $Cu\text{-}Ni/Al_2O_3$ catalyst can be due to the formation of a Ni–Cu alloy which could be formed. This Ni-Cu alloy may be responsible for blocking and decreasing the number of sites involved in the carbon formation.

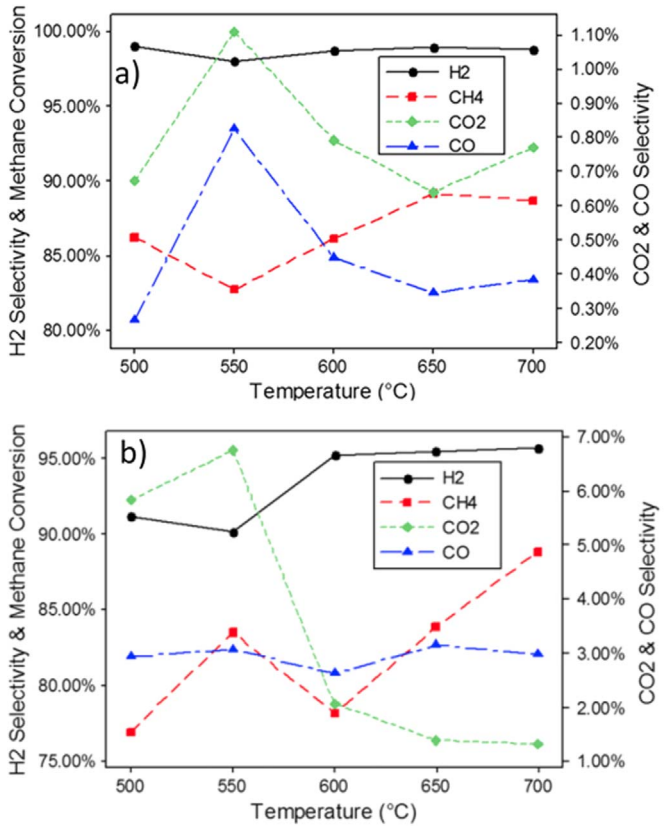

Fig. 5. Methane steam reforming over a) Ni–Cu/Al_2O_3 catalyst and b) Ni/Al_2O_3 catalyst [70].

MgO and Nb_2O_5 have both been employed as the additives for SRM in the Ni/Al_2O_3 catalyst. MgO as a support increases the CO_2 selectivity of the process at a steam to carbon (S/C) molar ratio of 2, Nb_2O_5 is well known for its acidic nature. Both MgO and Nb_2O_5 provide strong metal–support interaction. Amjad et al., [97] reported the use of MgO and Nb_2O_5 as the support for the Ru catalyst. Ru was introduced to the MgO and Nb_2O_5 support by the wet impregnation method before calcining at different temperatures. The Ru/Nb_2O_5 catalyst shows higher activity in terms of CH_4 conversion, CO_2 selectivity, and H_2 dry outlet concentration compared to MgO supported catalyst. The prepared catalyst showed different Ru oxidation states in XPS spectra depending on the preparation condition and precursor used.

Homsi et al. [83] studied the combination of MgO and Al_2O_3 supported Ru catalysts ($Co_xMg_{6-x}Al_2$) for SRM. The basic nature of MgO allows it to resist coking due to the enhancement in the oxidation rate of CH_x fragments which are adsorbed on the Ru active metal. The acidic nature of Al_2O_3 will facilitate the decomposition of methane. Four different $Co_xMg_{6-x}Al_2$ (x = 0, 2, 4 and 6) supports were prepared by the hydrotalcite route and Ru was introduced to the $Co_xMg_{6-x}Al_2$ support by wet impregnation method, this was then calcined at 500 °C. Fig. 6 shows the X-ray diffraction (XRD) spectra of $Ru\text{-}Co_xMg_{6-x}Al_2$ catalyst calcined in air at 500 °C. The supports with a high Mg content showed more intense RuO_2 diffraction lines with increased RuO_2 particle size. In the presence of high Co loading RuO_2 leads to the formation of smaller particles that are well dispersed on the Co_6Al_2 support making it non detectable by the XRD technique. At high Co loadings Ru interacts differently from that obtained with the Mg rich support. The SRM on Ru/Co_6Al_2 catalyst showed the highest H_2 molar concentration produced as well as the lowest CO concentration, demonstrating that Ru/Co_6Al_2 catalyst favors the water gas shift (WGS) reaction. The improved reactivity of high cobalt content catalyst is due to the result of improved surface properties of the support. An opposite behavior was

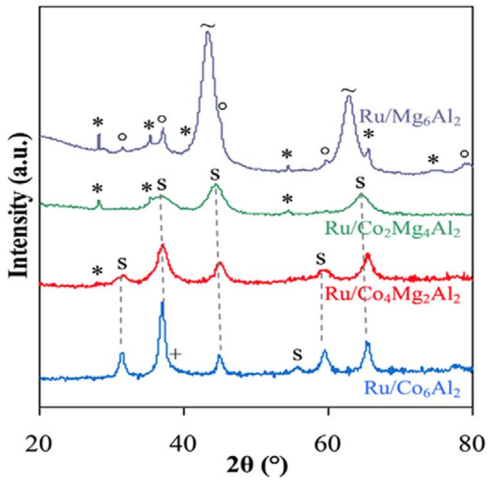

Fig. 6. XRD patterns ("s": $Co_3O_4/CoAl_2O_4/Co_2AlO_4$; "○": $MgAl_2O_4$; "~": MgO; "∗": RuO_2; "+":Co_2RuO_4) [83].

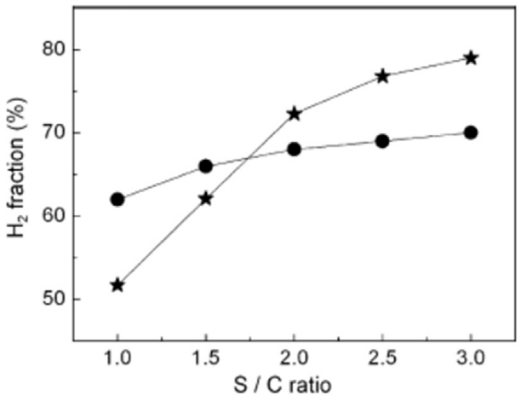

Fig. 7. H_2 fraction obtained using LCFN-0.2 (•) and commercial catalyst (★) for various S/C ratios at 700 °C [98].

observed for the Mg rich support as well as an intermediate behavior observed for $Ru/Co_4Mg_2Al_2$ and $Ru/Co_2Mg_4Al_2$ catalysts. Additionally, the Ru/Co_6Al_2 catalyst is stable for 100 h on stream.

Various transition materials like Ni, Co, Fe and noble metals like Pt, Rh, Pd, Ir, and Ru have been reported to be active for SRM. However, deactivation of the catalyst due to carbon deposition was a major problem. Perovskite oxides (ABO_3) have been studied as catalysts for the production of syngas from hydrocarbon fuels. Perovskite oxides generally contain rare-earth elements in A-site (like La, Sr, or Ba) which determines the thermal stability of the catalyst and B site is occupied by a 3d transition metal, such as Ni, Co, or Fe, which determines the catalytic activity for steam reforming. Perovskite-type oxides are widely studied due to their high stability under a wide range of oxygen partial pressures as well as their ability to form metallic particles in the order of the nanometers under reforming condition which diminish coke formation. Choi et al. [98] studied the SRM over $La_{1-x}Ce_xFe_{0.7}Ni_{0.3}O_3$ ($x = 0.1 \leq x \leq 0.5$) perovskite catalysts and compared their results with a commercial catalyst containing 10–14 wt% of NiO and 86–90 wt % of Al_2O_3. Fig. 7 shows the H_2 produced with $La_{0.8}Ce_{0.2}Fe_{0.7}Ni_{0.3}O_3$ (LCFN-0.2) and a commercial catalyst at 700 °C with different S/C ratios. The H_2 produced using the commercial catalyst decreased from 79% to 51.9% when the S/C ratio was decreased from 3 to 1, while the H_2 produced using LCFN-0.2 catalyst remain unaffected with the S/C ratio. The amount of coke formed on the commercial catalysts was 48.7 wt% and 0.2 wt% for LCFN-0.2 after a 20 h stability test. In the perovskite LCFN catalyst, lattice oxygen vacancies in the perovskite structure may be responsible for enhanced coke gasification of the carbon species formed over the catalyst. The oxygen vacancies also act as active sites for the dissociation of steam under the reaction condition.

Urasaki et al. [99] studied the SRM on Ni catalyst supported on a variety of perovskite oxides, including $LaAlO_3$, $LaFeO_3$, $SrTiO_3$, $BaTiO_3$, $La_{0.4}Ba_{0.6}Co_{0.2}Fe_{0.8}O_{3-\delta}$ (LBCF), and compared the catalytic activity and resistance to coking of perovskite catalysts to the conventional Ni/Al_2O_3 catalyst. Perovskite catalysts $LaAlO_3$, $LaFeO_3$, LBCF were prepared by the Pechini method and the catalysts were calcined at 850 °C for 11 h. $SrTiO_3$ and $BaTiO_3$ catalyst were prepared by solid state reaction at 1150 °C for 10 h. 10 wt% Ni was introduced in the perovskite catalyst by impregnation using an aqueous solution of $Ni(NO_3)_2{\cdot}6H_2O$. Fig. 8 shows the activities of various Ni/perovskite catalysts and the conventional Ni/Al_2O_3 catalyst in SRM tested at 800 °C with a steam to methane ratio of 2. The catalytic activity of $Ni/LaAlO_3$ and $Ni/SrTiO_3$ catalyst were comparable to that of the conventional Ni/Al_2O_3 catalyst. Meanwhile, the catalytic activity of $Ni/LaFeO_3$ showed a lower activity while the activities of $Ni/BaTiO_3$ and Ni/LBCF were also extremely poor. The $Ni/LaAlO_3$ and $Ni/SrTiO_3$ catalyst showed CH_4 conversion levels of 91.7% and 88.4% after being run for 1 h, respectively. Temperature programed reduction (TPR) studies showed that a larger amount of lattice oxygen is removed from $Ni/BaTiO_3$ during reduction

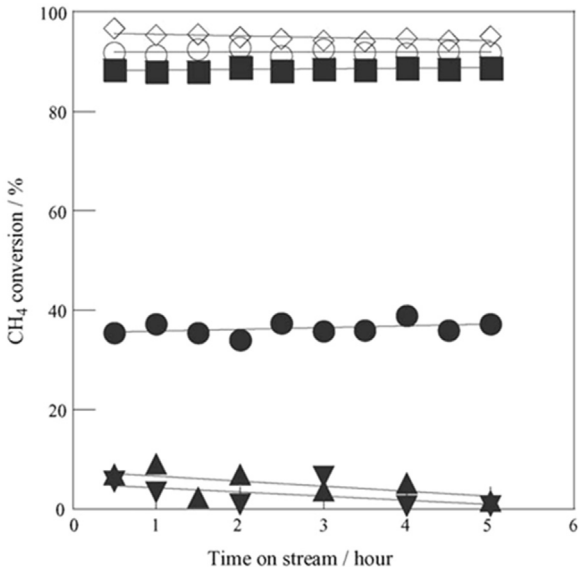

Fig. 8. Catalytic activities of supported Ni catalysts. Catalyst; (○) $Ni/LaAlO_3$, (■) $Ni/SrTiO_3$, (•) $Ni/LaFeO_3$, (▲) $Ni/BaTiO_3$, (▼) Ni/LBCF, (◇) Ni/Al_2O_3. Reaction conditions: temperature, 800 °C; molar H_2O/CH_4 ratio, 2 [99].

with hydrogen when compared with either the $Ni/LaAlO_3$ or $Ni/SrTiO_3$ catalyst. This explains why the $Ni/LaAlO_3$ and $Ni/SrTiO_3$ catalysts displayed higher catalytic activities than $Ni/BaTiO_3$, because $LaAlO_3$ and $SrTiO_3$ catalysts have a larger amount of lattice oxygen near the surface and metallic nickel. The lattice oxygen present close to active nickel sites can be easily transferred to CH_x fragments adsorbed on metallic nickel, which facilitates the oxidation of CH_x fragments. Therefore, transition element based perovskite oxides are promising anti-coking catalysts for the reforming of hydrocarbons.

It should be noted that there is a process which combines steam-reforming of methane and CO_2 absorption together in a single reaction step over a steam reforming catalyst mixed with a CO_2 absorbent. This process is called sorption-enhanced H_2 production. The removal of the produced CO_2 from the system by the solid absorbent makes reaction (4) shift to the right thus methane conversion will be enhanced. The produced H_2 can have a purity of 98% with only a small amount (ppm level) of CO and CO_2 thus minimizing the requirement on purification. However, the CO_2 absorbent may be saturated after a period of time thus regeneration is required which can be achieved through temperature or/and pressure swing. The sorption-enhanced H_2 production has been covered by a few excellent reviews [100–105]. The key challenge is the multicycle durability of CO_2 absorbent which must be improved [101].

Hydrogen production through chemical looping was also investigated. In 1993, Steinfeld and Kuhn proposed to production hydrogen through combining methane and solar thermal with the use of Fe produced from Fe_3O_4 as the reaction catalyst [106].

First, methane reacts with Fe_3O_4 to form Fe, H_2 and CO according to the following reaction,

$$Fe_3O_4 + 4CH_4 = 3Fe + 8H_2 + 4CO \quad (5)$$

The molar ratio of produced CO and H_2 is 1:2 which can be used as an important intermediate for the gasto-liquids (GTL) process for the production of liquid hydrocarbons [107].

In the following step, steam is introduced to the system to react with the produced Fe, forming pure H_2,

$$4H_2O + 3Fe = Fe_3O_4 + 8H_2 \quad (6)$$

The advantage of this chemical-looping H_2 production is that a gas separation process is not required. The produced pure H_2 and syngas in the individual step are both very useful chemical products. Chemical

Table 3
Chemical composition of Ni-metal/support catalyst and noble metal/support for partial oxidation of methane.

Catalyst	Preparation method	Temperature (°C)	Weight hour space velocity (ml h^{-1} g_{cat}^{-1})	O_2 to carbon ratio (O/C)	Conversion (%)	H_2 selectivity (%)	Ref.
M/Mg/Al M = Rh, Ni, Rh/Ni, Ir/Ni or Ru/Ni	co-precipitation	750	339,292	0.5	92	40	[115]
Pt/Ni/Al_2O_3 Pt	impregnation	800	225,000	0.5	85	NA	[116]
M + Ni/Al_2O_3 M = Ru, Rh, Pd, Pt	impregnation	800	90,000	0.5	> 80	> 90	[117]
Pt-NiO/Al_2O_3	impregnation	800	7200	0.5	91.8	98.4	[118]
M/Ni/Al_2O_3 M = Ru, Pd, Pt	Precipitation/ impregnation	800	560,000	0.5	> 80	90	[119]
Co/Al_2O_3	impregnation	850	60,000	0.5	95	93.6	[120]
Pt–Co/Al_2O_3	impregnation	750	56,000	0.4	95	NA	[121]
Ni/ 12CaO·7Al_2O_3	solid-state reaction/ impregnation	800	30,000	0.5	> 90	> 95	[122]
Pt/12CaO·7Al_2O_3	solid-state reaction/ impregnation	800	30,000	0.5	> 90	> 90	[122]
Ni-Co/$CaAl_2O_4$/Al_2O_3	impregnation	800	144,000	0.5	90	> 95	[123]
Co/MgO	impregnation	850	20,000	0.5	95		[124]
Co/ZrO_2	impregnation	800	60,000	0.5	100	98.1	[125]
Co/La_2O_3	impregnation	800	60,000	0.5	97.4	96.6	[125]
NiCoMgCeO_x/ZrO_2-HfO_2	impregnation	800	62,000	0.55	95	95	[126]
NiCoMgO_x/ZrO_2-HfO_2	impregnation	850	62,000	0.55	95.5	98.5	[127]
NiCo/SBA–15	hydrothermal/ impregnation	700	5000	0	NA	> 40	[128]
LiNiLaO_x//Al_2O_3	impregnation	850	27,000	0.5	97	NA	[129]
Ni/CeO_2/Al_2O_3	impregnation	800	152,432	0.5	80.3	NA	[130]
NiO/La_2O_3/γ-Al_2O_3	impregnation	750	110,000	0.5	94.3	98	[131]
LiLaNiO/Al_20_3	impregnation	850	270,000	0.5	> 90	> 95	[132]
Ni–Cr/Al_2O_3	impregnation	700	195,000	0.5	85	NA	[133]
NiFe-ZrO_2/Cu	combustion/ impregnation	800	28,500	0.5	> 60	NA	[134]
Ir-Ni/Al_2O_3	impregnation	600	88,500	0.5	80		[135]
Pt-Ni/Al_20_3	impregnation	800	500,000	0.55	88.1	97.5	[136]
Ni–Pt/$La_{0.2}Zr_{0.4}Ce_{0.4}O_x$	combustion	700	480,000	0.5	> 80	NA	[137]
Pt/$Ni_{0.5}$/MgAlOx	impregnation	750	3,000,000	0.5	> 90	NA	[138]
Cu-Ni/$Ce_{0.9}Zr_{0.1}O_2$	combustion/ impregnation	750	532,121	0.38	> 30	NA	[139]
Rh-CeO_2	hydrothermal	700	60,000	0.5	95.2	92.9	[140]
Ni-Rh/Al_2O_3–MgO	coprecipitation	750	354,044	0.5	93	95	[141]
Rh/Ni/Mg/Al hydrotalcite	coprecipitation	750	111,357	0.5	90	> 95	[142]
Ni/SiC	Sol-gel/ impregnation	750	20,000	0.5	> 75	> 95	[143]
Ni/ZrO_2@SiO_2 core shell	Stober method	750	50,000	0.5	> 90	> 75	[144]
Ni/CeO_2	Precipitation/ impregnation	750	50,000	0.5	> 85	> 65	[145]
Ni/zeolite catalysts	impregnation	750	90,000	0.5	100	NA	[146]
Ni/CeO_2–La_2O_3	impregnation	800	60,000	0.5	> 90		[147]
Ni/CeO_2-Al_2O_3	Pechiney	750	12,000	0.5	> 80	> 90	[148]
Ni/TiO_2	impregnation	800	4800	0.5	86.3	99.7	[149]
Ni-M/Anodic TiO_2 M = Ru, Pt, Rh	impregnation	700	30,000	0.5	> 70	> 70	[150]
NiO-Al_2O_3	Sol-gel	600	50,400	0.5	> 75	> 75	[151]
$LaCoO_3$/γ-Al_2O_3	combustion	800	899,550	0.25	> 35	> 40	[152]
$NdCaCoO_{3.96}$	solid-state reaction	915	20,000	0.48	> 75	> 90	[153]
$Sr_{0.8}Ni_{0.2}ZrO_3$	hydrothermal	900	66,000	0.5	> 94	NA	[154]
$La_{0.08}Sr_{0.92}Fe_{0.20}Ti_{0.80}O_3$	Pechiney	900	30,000	0.5	> 50	> 60	[155]
$La_{0.5}Sr_{0.5}CoO_3$	Sol-gel	850	30,000	0.5	> 70	> 75	[156]
$Gd_{0.33}Ba_{0.67}FeO_3$	Pechiney	950	73,600	0.13	94		[157]
Ni@SiO_2 core shell		700	72,000	0.5	83.9	85.9	[158]
$La_{0.3}Sr_{0.7}Fe_{0.7}Cu_{0.2}Mo_{0.1}O_3$ membrane reactor	combustion	900	848	0.51	> 80	> 70	[159]
La_2NiO_4 membrane reactor	solid-state reaction	900	5940	0.5	89	NA	[160]
$Yb_2Ru_20_7$	solid-state reaction	777	22,400	0.5	83	95	[161]

looping H_2 production has been reviewed by Tang et al. [108]

There are some key reports in chemical-looping production of hydrogen using Fe_2O_3-CeO_2 as the oxygen carrier [107,109,110]. The key challenge is carbon deposition when the oxide reacts with methane therefore making reaction (5) incomplete. Sintering of the formed Fe is another problem [107]. The weak oxidation ability of H_2O leading to a low oxidation degree and slow oxidation rate also remain as challenges [108]. It is therefore very important to find suitable oxygen carriers which have a good reactivity and high agglomeration resistance for this process. It was found that perovskite oxides $LaFe_{1-x}Co_xO_3$ are good oxygen carriers for the chemical looping steam methane reforming to syngas and hydrogen co-production [111]. Another strategy to prevent sintering and improve the stability of the catalyst has been the introduction of pores into the oxygen carrier. It has been reported that macroporous CeO_2-ZrO_2 solid solutions are excellent oxygen carrier for chemical-looping stream reforming of methane [112].

Both sorption-enhancement and chemical looping H_2 production are very attractive due to gas separation being minimized or not required at all, however, there are challenges that must be overcome before any real applications can be achieved.

3.2. Partial oxidation of methane for hydrogen production

Partial oxidation, in which methane, natural gas or a hydrocarbon is heated in the presence of a stoichiometric amount of pure oxygen, has attracted a lot of attention in recent years. Partial oxidation of methane shows several advantages over steam reforming including; good response time, compactness, and less sensitivity for fuel variation. Partial oxidation reactors are gaining increased interest in the energy conversion field particularly in high temperature fuel cells. Partial oxidation of methane is a highly exothermic reaction and is considered as a faster reaction than the SRM [113].

$$C_nH_m + \frac{1}{2}nO_2 \rightarrow nCO + \frac{m}{2}H_2 \quad (7)$$

The partial oxidation of hydrocarbon to syn-gas (CO + H_2) can occur at very high temperatures without the use of a catalyst; however, the operating temperature will be significantly reduced with the use of catalysts.

Partial oxidation of methane (POM) to fuel rich syn-gas can be represented as,

$$CH_4 + \frac{1}{2}O_2 \rightarrow CO + 2H_2 \quad \Delta H^{\circ}_{298\,K} = -35.6\ \text{kJ mol}^{-1} \quad (8)$$

The most studied catalysts for POM are similar to steam reforming catalysts including supported transition metals (Ni, Co, and Fe), noble metals and perovskite oxides [114]. Although, transition metals are active catalyst components for POM, the metal species with different oxidation states plays a significant role in the methane conversion steps. When referring to a Ni supported catalyst, metallic nickel is used to promote the formation of syn-gas, and the Ni species with oxidation number ≥2 will promote the total combustion of methane. In general, the distribution of the catalyst metallic species with various oxidation states depends on the synthesis process and the support properties. Table 3 summarizes the different catalyst systems investigated in the literature. In the reported catalysts, Co/ZrO_2 is an excellent low cost catalyst with both high conversion and H_2 selectivity [98].

Pantaleo et al. [147] studied the POM of a Ni catalyst supported over CeO_2, La_2O_3 and mixed CeO_2-La_2O_3. The Ni catalyst supports were prepared by co-precipitation and wet impregnation. During stability tests it was observed that carbon formed only on the single oxide supported catalysts, Ni/CeO_2 and Ni/La_2O_3. In the presence of mixed supports like CeO_2-La_2O_3 carbon did not formed, this was due to the formation of different nickel–lanthanum oxide species with different Ni oxidation states. It was also reported that the defect species over the support play an important role in the POM by Pal et al. [145]. Fig. 9 shows the schematic representation of Ni/CeO_2 and CeO_2 surface showing surface defects with under coordinated oxygen atoms. When the Ni content is low (i.e., up to 2.5% Ni) in CeO_2, the defects are mainly substitution defects. The enhancement of the interstitial and surface (structural) defects by the formation of the –O-Ni-O-Ce super structure with exposure to highly under-coordinated O atoms can be achieved by further increasing the Ni content in CeO_2. These under-coordinated O atoms strongly interact with the C–H bond facilitating the cleavage of weakened C–H bonds, while the pure CeO_2 shows a lower affinity of CH_4 toward the “Ce center”, due to absence of point defect and surface defects.

Abbasi et al. studied the monolith supported noble metal (Pt, Pt:Pd, and Pd) catalyst for POM [162]. The results of the POM test showed that the most active catalyst for both wet and dry feeds was Pd, which was followed in order of decreasing activity by Pt:Pd and then by Pt. Santis-Alvarez et al. investigated the effect of different supports (Al_2O_3 and $Ce_{0.5}Zr_{0.5}O_2$) on a Rh based catalyst [163]. It was found that Rh oxidation was inhibited by the Al_2O_3 support and POM over $Rh/Ce_{0.5}Zr_{0.5}O_2$ catalyst support was limited due to continuous re-oxidation of metallic Rh by oxygen spillover from the support.

Among studied catalysts for POM, it was found that perovskite based catalyst materials exhibited good catalytic activity, good stability and the ability to restrain itself from carbon deposition. It has been claimed that the perovskite catalyst can be used to bring down the threshold value needed to generate the carbon deposition. Carbon deposition can also be prevented through the reaction of the oxygen species over the perovskite reacting with the carbon deposition. Staniforth reported a $Sr_{0.8}Ni_{0.2}ZrO_3$ perovskite catalyst with high selectivity and activity for POM [154]. Fig. 10 shows the stability of this $Sr_{0.8}Ni_{0.2}ZrO_3$ perovskite catalyst for different cycles at a temperature of 900 °C. Catalyst deactivation was not observed during the stability test with a high stability of the $Sr_{0.8}Ni_{0.2}ZrO_3$ perovskite catalyst shown for the reducing environment at 900 °C. A similar result was also reported by Meng et al. when using a $LaGa_{0.65}Mg_{0.15}Ni_{0.20}O_3$ (LGMN) perovskite catalyst for the partial oxidation of methane to syngas [114]. The LGMN perovskite catalyst syngas selectivity reached up to 100% with the methane conversion reaching values larger than 81% at 900 °C. Post analysis test on the catalyst after POM showed that the LGMN catalysts contain a major perovskite phase and other phases like La_2O_3, $La_2O_2CO_3$ along with metallic Ni.

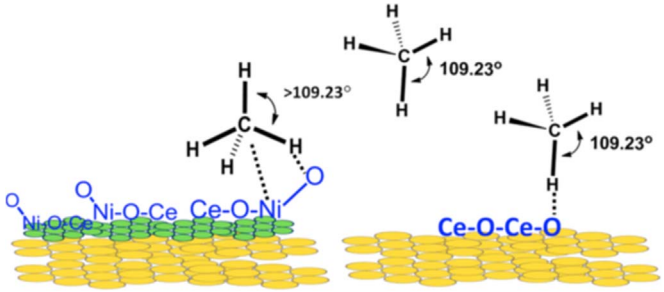

Fig. 9. Schematic representation of Ni/CeO_2 and CeO_2 surface having surface defects with under coordinated oxygen atoms [145].

3.3. CO_2 reforming of methane for hydrogen production

Dry reforming of methane (DRM) with CO_2 is very attractive in terms of syngas production as it can be used to convert greenhouse gases (CH_4 and CO_2) into valuable fuel rich syngas for both domestic and industrial utilization. In the dry reforming process carbon dioxide is used to reform methane to obtain syngas (H_2 and CO) by the following reaction:

$$CH_4 + CO_2 \rightarrow 2H_2 + 2CO \quad \Delta H^{\circ}_{298\,K} = 247\ \text{kJ mol}^{-1} \quad (9)$$

In reality the above reaction proceeds through a number of complex intermediate steps involving absorption, disproportionation, recombination and desorption. These intermediate reactions typically

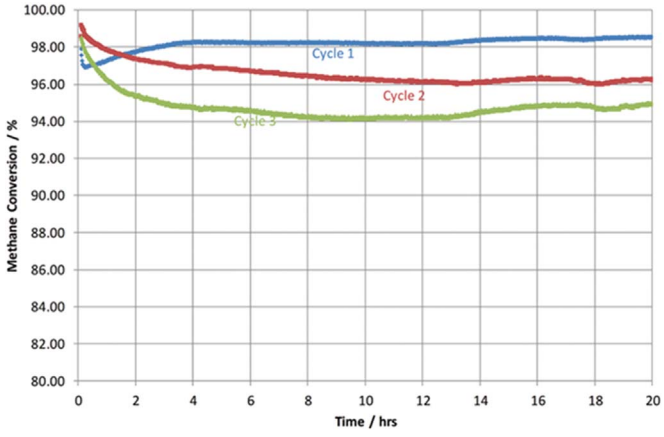

Fig. 10. Methane conversion during reaction of methane and limited oxygen (CH_4:O_2 = 2) over $Sr_{0.8}Ni_{0.2}ZrO_3$ for different cycles at a reaction temperature of 900 °C [154].

Table 4
Chemical composition of metal/support catalyst used for dry reforming of methane.

Catalyst	Temperature (°C)	Weight hour space velocity (ml h^{-1} g_{cat}^{-1})	CO_2 to carbon ratio (CO_2/C)	Conversion CH_4 (%)	Conversion CO_2 (%)	H_2/CO ratio	Ref.
2% Cr–40% Ni/CeO_2	850	10,200	1	90	95	NA	[169]
Ni-Pt/Al_2O_3	700	7500	1	65	76	0.65	[170]
5%Ni/$Ce_{0.8}Pr_{0.2}O_2$	750	30,000	1	71.5	83.4	1.20	[171]
Ni/SBA–15	650	52,800	1	98	86	1.09	[165]
Ir/$Ce_{0.9}Pr_{0.1}O_2$	750	18,000	1	61.1	74.5	0.97	[172]
Ni/CeO_2-TiO_2	800	14,400	1	> 80		0.73–0.82	[173]
Ni-Al_2O_3	800	72,000	1	> 85	> 85	NA	[174]
Ni-Mo_2C/La_2O_3	800	12,000	1	60	80	NA	[175]
Ni@SiO_2	750	40,000	1	71.2	58.4	0.75	[166]
Ni-Ce/$MgAl_2O_4$	700	10,000	1	> 90	> 90	NA	[176]
$Ni_{17}W_3$ alloy/ SiO_2	800	96,000	1	60	70	NA	[177]
Co-Ce/ZrO_2	700	20,000	1	> 70	NA	> 0.6	[178]
Co/CeO_2	750	30,000	1	79.5	87.6	NA	[179]
$NiMg_xAl_y$	800	80,000	1	80	95	NA	[180]
$NiPt_x/Al_2O_3$	700	20,000	1	87.2	90	0.96	[181]
Co-Zr/Activated Carbon	750	7200	1	90.6	88.5	NA	[182]
Pt/PrO2–Al2O3	650	48,000	1	67.3	79.2	0.84	[183]
Rh/CaO-SiO_2	650	222,222	1	11.8		0.53	[184]
4% Ni–0.2% Au 0.2% Pt–10% CeO_2	800	60,000	1	93.41	97.26	NA	[185]
Ni/$CeAlO_3$-Al_2O_3	800	20,000	1	80	90	NA	[186]
NiO-MgO-ZrO_2	750	64,500	0.67	65	75	NA	[187]
$La_{1-x}Sr_xCoO_3$	800	24,000	1	93.6	98.9	NA	[188]
$LaNi_xFe_{1-x}O_3$	800	300,000	1	80	NA	0.95	[189]
Ni-$Ce_{0.8}Zr_{0.2}O_2$	750	44,800	0.92	73.2	85	NA	[190]
$La_{0.9}Ba_{0.1}NiO_3$	700	24,000	1	50	55	0.66	[191]
Rh-CeO_2	750	11,100	1	48.6	57	0.73	[192]
Ni-Ba/Al_2O_3	700	30,000	1	60	70	0.6	[193]
Ru/$Ce_{0.7}5Zr_{0.25}O_2$	900	12,000	1	96	98	1	[194]
Rh-Ni/ Boron Nitride	700	60,000	1	72	81	0.7	[195]
$M_xLa_{1-x}Ni_{0.3}Al_{0.7}O_3$ M = Li, Na,K	750	15,000	1	90	NA	1	[196]
$La_{0.95}Ce_{0.05}NiO_3$	750	72,000	1	50	60	0.4	[197]
$LaNi_{1-x}Mg_xO_3$	700	600,000	1	57	67	0.47	[198]
$LaNi_{0.8}Ru_{0.2}O_3$	750	72,000	1	80	85	0.6	[199]
$Ce_2Zr_{1.51}Ni_{0.49}Rh_{0.03}O_8$	800	12,000	1	30	100	NA	[200]
$LaNi_{0.95}Rh_{0.05}O_3$	650	40,000	1	70	NA	NA	[201]
Pt -Ni/nanofibrous-Al_2O_3	700	30,000	1	> 65	> 70	NA	[202]
Rh/Al_2O_3	800	60,000	1	56.9	NA	NA	[203]

influence the DRM reaction by the reverse water gas shift (RWGS) reaction, which leads to a H_2/CO ratio different from less than unity.

$$CO_2 + H_2 \leftrightarrow CO + H_2O \quad \Delta H^{\circ}_{298\,K} = 41.2\ \text{kJ mol}^{-1} \tag{10}$$

In addition to the difficulties associated with the RWGS reaction DRM has the inherent disadvantage of rapid catalyst deactivation due to carbon buildup on the catalyst surface. Coke deposition can be either formed by methane decomposition and/or by CO disproportionation reaction (Boudouard reaction) to form solid carbon on the catalyst surface producing H_2.

$$CH_4 \rightarrow C + 2H_2 \quad \Delta H^{\circ}_{298\,K} = 75\ \text{kJ mol}^{-1} \tag{11}$$

$$2CO \leftrightarrow C + CO_2 \quad \Delta H^{\circ}_{298\,K} = -171\ \text{kJ mol}^{-1} \tag{12}$$

Therefore to reduce coke deposition in the DRM reaction the use of a catalyst system that effectively reduces this is required. The use of Ni and Co based catalysts is a preferable choice due to their abundance, high activity and the economically feasible cost. However, the Ni catalyst suffers from rapid deactivation and coke formation. Different type catalysts such as, Ni, Ru, Rh, Pd, Ire, Pt or Co, on a oxide support, such as SiO_2, Al_2O_3, MgO, TiO_2, CaO, CeO_2, ZrO_2, or La_2O_3 have been studied for DRM in order to overcome the coke formation [164]. Table 4 summarizes the chemical composition of metal/support catalysts and noble metal/supports for DRM. Among the investigated, Ni/SBA-15 is a promising one with high CH_4 and CO_2 conversion plus high H_2 to CO ratio [165].

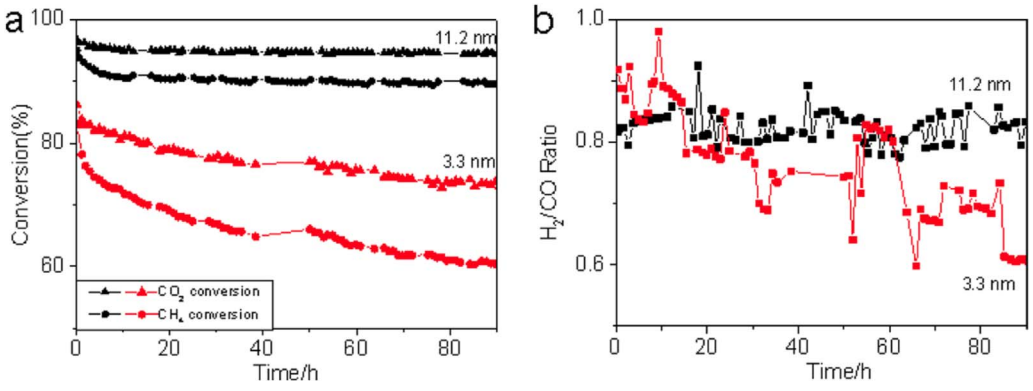

Fig. 11. Stability test for Ni@SiO_2 with 3.3 nm and 11.2 nm shell thickness. Conditions: 800 °C, GHSV = 36,000 ml g^{-1} cat h^{-1}, CO_2:CH_4:N_2 = 1:1:1 [167].

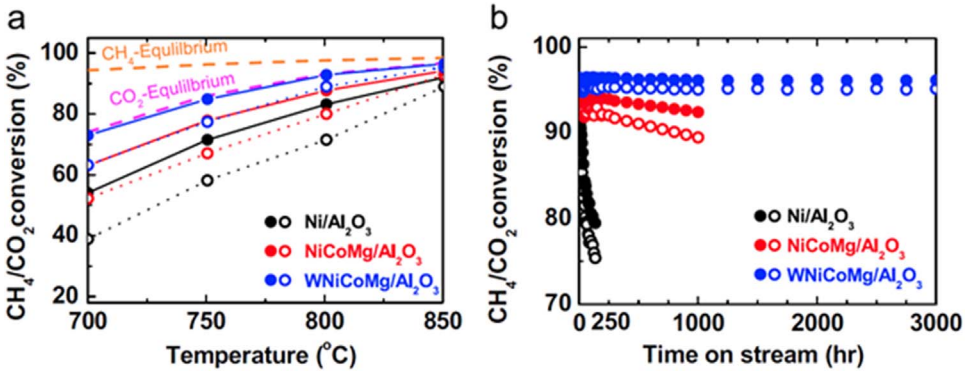

Fig. 12. CH_4 and CO_2 conversion efficiency as a function of temperature (700–850 °C) for various Ni-based Al_2O_3 catalysts (Ni/Al_2O_3, NiCoMg/Al_2O_3, and WNiCoMg/Al_2O_3), (b) long-term stability of CH_4 and CO_2 conversion of catalysts up to 3000 h at 850 °C (Reaction conditions: P = 1 atm, CH_4:CO_2:N_2 = 1.0:1.0:1.0, GHSV = 80,000 h^{-1}) [168].

Effective stabilization of the metal catalyst against coke formation can be achieved through percolating the metal catalyst with inorganic layers such as SiO_2 and Al_2O_3. A new Ni@SiO_2 core shell catalyst introduced by Zhang et al. to study the DRM shows a stable performance by reducing the formation of coke on the catalyst surface [166]. Similarly, Li et al. studied the effect of shell thickness with Ni@SiO_2 catalyst towards DRM [167]. It was found that a small increase in the shell thickness of the Ni@SiO_2 catalyst results in dramatic improvements in catalyst stability and specific activity towards CH_4 and CO_2. Fig. 11 shows the stability test for Ni@SiO_2 with 3.3 nm and 11.2 nm shell thickness at 800 °C. The high catalytic activity of Ni@SiO_2 was due to the effective void space between the Ni core and the SiO_2 shell providing a uniform reaction environment which improves the adsorption ability of Ni towards methane.

Addition of basic metal oxide supports to the DRM (eg: MgO) catalyst provide a promising alternative to minimize carbon deposition. The basicity of these supports and/or promoters will bring a more favorable CO_2 adsorption through the formation of bicarbonate (HCO_3^-) or carbonate species (CO_3^{2-}) were the CO_2 interacts with basic OH surface species or O^{2-} surface ions. Son et al. reported a high carbon resistant MgO promoted NiCo/Al_2O_3 catalyst (WNiCoMg/Al_2O_3) with a $MgAl_2O_4$ nano island decorated on the DRM catalyst [168]. Fig. 12 shows the performance of Ni/Al_2O_3, NiCoMg/Al_2O_3, and WNiCoMg/Al_2O_3 catalyst at atmospheric pressure using high gas hourly space velocity (GHSV) of 80,000 h^{-1} showing an excellent stability over 3000 h. The excellent catalytic activity and long term stability of WNiCoMg/Al_2O_3 catalyst mainly originates from the robust structure of the catalyst itself.

4. Reforming of liquid hydrocarbons for hydrogen production

The production of hydrogen from liquid hydrocarbons such as ethanol, methanol, etc. has received considerable research attention due to their economic importance and environmental benefits [204,205]. Unlike SRM, steam reforming of liquid hydrocarbons involves complex pathways and intermediate products which depend on the nature of the metal surface. For example ethanol steam reforming (ESR), commonly reported surface intermediated species [206] such as acetaldehyde (CH_3CHO*), acetyl (CH_3C*O), ketene (*CH_2C*O), and ketenyl (*CHC*O) and other intermediate species like *CHyCHx*OH and *CH_2CH_2O* are formed on the metal catalyst surface. Their molecular structures are shown in Fig. 13. Similarly, the commonly identified surface intermediate species [207] formed during methanol steam reforming (MSR) are methoxy (*OCH_3), formaldehyde (*OCH_2), dioxymethylene (*OCH_2O*), mono-dental formate (*OCHO), bidental formate (*OCHO*), and methyl formate (*$OCHOCH_3$). Their molecular structure is shown in Fig. 14. Table 5 summarizes the chemical composition of the Ni-metal/support catalyst and noble metal/support for steam reforming of liquid hydrocarbons. Among the investigated catalysts, Cu-based catalysts are the best in terms of cost and conversion.

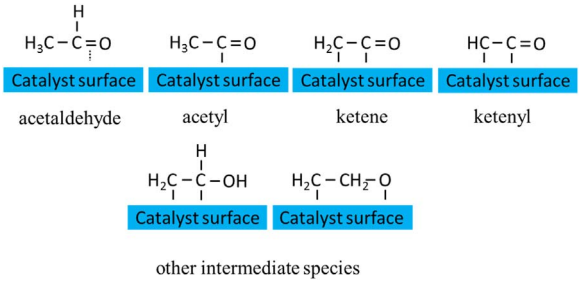

Fig. 13. Representation of intermediate species molecular structures of ethanol steam reforming on catalyst surfaces.

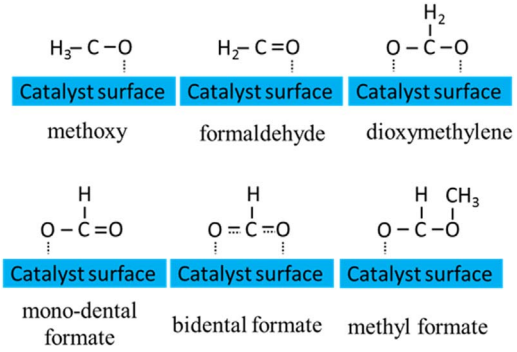

Fig. 14. Representation of intermediate species molecular structures of methanol steam reforming on catalyst surfaces.

4.1. Reforming of methanol for H_2 production

Experimental studies of MSR carried out on Ni-Cu/ZrO_2 catalyst have been reported by Lytkina et al. [208] using different Ni and Cu ratios and annealing temperatures. ZrO_2 was prepared by the precipitation method and the resulting samples were sequentially impregnated with aqueous solution of Cu and Ni. The obtained bi-metallic catalysts were further annealed at 350 and 400 °C followed by reduction at 350 °C in H_2. Four catalyst supports prepared with different Cu/Ni ratios and at different temperatures were produced. (1). $Cu_{0.8}$-$Ni_{0.2}$/ZrO_2 350 °C; 2) $Cu_{0.2}$-$Ni_{0.8}$/ZrO_2 400 °C; 3) $Cu_{0.8}$-$Ni_{0.2}$/ZrO_2 400 °C; 4) $Cu_{0.2}$-$Ni_{0.8}$/ZrO_2 350 °C. Thermal analysis (DSC) and XRD patterns shows that the catalyst annealed at 350 °C is amorphous whereas the catalyst annealed at 400 °C has a monoclinic structure. For all compositions of the catalyst support a methanol conversation was archived at over 350 °C. Fig. 15 shows the temperature dependence of hydrogen formation on different Ni-Cu/ZrO_2 catalysts. The catalyst annealed at 350 °C (amorphous) shows higher hydrogen production compared to catalyst annealed at 400 °C (monoclinic). It is well known that water absorption on the catalyst surface plays an important role in reforming reactions. The increase in H_2 production on the $Cu_{0.8}$-$Ni_{0.2}$/ZrO_2 350 °C

Table 5
Chemical composition of Ni-metal/support catalyst and noble metal/support for steam reforming of liquid hydrocarbon.

Catalyst	Fuel	Preparation method	Temperature (°C)	Weight hour space velocity (ml h^{-1} g_{cat}^{-1})	Steam to carbon ratio (S/C)	Conversion (%)	H_2 selectivity (%)	Ref.
$CuNi/CeO_2$	ethanol	impregnation	450	57,000	10	60	70	[219]
Cu/ZnO	methanol	homogeneous precipitation	250	12,600	1.2	100	NA	[227]
CuZnZrAl	methanol	impregnation	350	903	1.4	> 50		[228]
Cu–Mn spinel	methanol	soft reactive grinding	260	10,080	1.3	92.9	99.5	[229]
Cu/ZnO	methanol	soft reactive grinding	300	7680	1.3	100	60	[230]
$Cu/ZnO/ZrO_2/Al_2O_3$	methanol	precipitation	260	60,000	1.3	> 90	NA	[231]
$ZnO/Cu/SiO_2$	methanol	hydrolysis/ polymerization	300	21,200	1.5	> 75	NA	[232]
$CuO/ZnO/CeO_2/ZrO_2/Al_2O_3$	methanol	precipitation	270	22,909	1.1	90.5	NA	[233]
$Cu/ZnO/ZrO_2/Al_2O_3$	methanol	precipitation	300	276,000	1.3	100	NA	[234]
Cu–Zn–Ce–Al-oxide	methanol	impregnation	260	7331	1.4	90		[235]
$Ce_{1-x}Cu_xO_2$	methanol	precipitation	260	5000	1	90.7		[236]
$Cu_xMn_{3-x}O_4$ spinel	methanol	combustion	280	14,008	1.5	100	94.3	[237]
Ni/La_2O_3-ZrO_2	ethanol	impregnation	350	9180	30	100	55	[225]
Ni/CeO_2-ZrO_2	ethanol	impregnation	650	5517	8	100	> 75	[238]
Ni/GDC	ethanol	hydrothermal/ impregnation	850	80,000	3	100	65	[239]
Ni/TiO_2	ethanol	precipitation/ impregnation	500	29,160	3	99.5	NA	[240]
$Ni_{0.95}Mo_{0.05}$/SBA	ethanol	hydrothermal	700	8571	3	80	80	[224]
$CuNi/SiO_2$	ethanol	impregnation	350	17,177	6	100		[241]
$PtNi/CeO_2$	ethanol	hydrothermal/ impregnation	500	36,000	3	69	NA	[242]
$Pt_{1.5}Co_x/ZrO_2$	ethanol	sol-gel/impregnation	300	22,000	13	100	NA	[243]
$Ni_3Mg_2AlO_Y$	bio ethanol		300	168,000	3	100	60	[244]
Co_2MnO_4	ethanol	combustion	700	8571	0.33	100	71	[245]
$2KCo/ZrO_2$	ethanol	impregnation	420	60,000	9	100	74	[246]
$La_{0.6}Sr_{0.4}CoO_3$	ethanol	sol–gel citrate	700	40,000	3	100	70	[221]
$La_{1-x}Ca_xFe_{0.7}Ni_{0.3}O_3$	ethanol	pechini method	650	400,000	3	100	65	[247]
$La_{1-x}K_xFe_{0.7}Ni_{0.3}O_3$	ethanol	pechini method	450	60,000	3	100	70	[248]
$LaCo_xNi_{1-x}O_3$	ethanol	pechini method	550	60,000	3	100	60	[249]
$Ni/LaFe_{0.7}Co_{0.3}O_3$	ethanol	pechini	550	80,000	3	100	67	[250]
$Mn/Co_{10}Si_{90}$MCM	ethanol	hydrothermal/ impregnation	600	8571	0.33	100	97	[251]
$Rh/La_2O_3(5\%)CeO_2$–Al_2O_3	ethanol	impregnation	500	82,200	3	70	70	[215]
Rh/CeO_2	ethanol	deposition-precipitation	650	381,703	3	100	72	[211]
Ir/CeO_2	ethanol	deposition–precipitation	650	6000	1.8	100	55	[252]
Ir/CeO_2	ethanol	deposition–precipitation	450	22,000	4	100	NA	[253]
$Ir/Ce_{0.9}Pr_{0.1}O_2$	ethanol	impregnation	450	18,000	3	95	60	[254]
$Rh\text{-}Co/CeO_2$	ethanol	impregnation	450	72,000	3	90	60	[212]
Rh/MgO	ethanol	impregnation	650	24,000	8.4	100	92	[255]
Pt/CeO_2	bio ethanol	impregnation	350	25,350	3	82		[256]
$Pt/CeZrO_2$	ethanol	precipitation/ impregnation	500	80,000	0	100	> 50	[257]

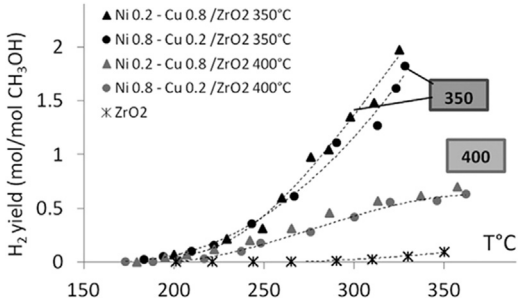

Fig. 15. Temperature dependence of H_2 yields in MSR on obtained catalysts [208].

catalyst may likely be due to the significantly higher content of water molecules absorbed on the surface of amorphous ZrO_2 catalyst than monoclinic ZrO_2 catalyst.

Besides oxides, carbides have also been investigated as the catalyst supports for reforming of liquid hydrocarbons Ma et al. studied the catalytic activity of metal modified Mo_2C catalysts for MSR with different M/Mo molar ratios [209]. The catalyst were prepared by mixing aqueous solutions of $(NH_4)_6Mo_7O_{24}{\cdot}4H_2O$, $Ni(NO_3)_2{\cdot}6H_2O$, $Fe(NO_3)_3{\cdot}9H_2O$ and $Co(NO_3)_2{\cdot}6H_2O$, respectively and calcining at 500 °C. Carburization of M–MoO_3 to M-Mo_2C was carried out in a fixed-bed quartz microreactor with a CH_4/H_2 (20 vol% CH_4) atmosphere. The MRS of Ni-Mo_2C with different doping amount of Ni (Ni/Mo ratio = 0.8/99.2, 1.2/98.8, 1.6/98.4, 2.4/97.6, 5/95, 10/90, and 15/85) was shown in Fig. 16. The catalytic performance of Ni-Mo_2C has a strong dependence on the methanol conversion. When the Ni loading is low (Ni/Mo = 0.8/99.2–2.4/97.6) the catalyst exhibits the highest methanol conversion with a reaction temperature of 300 °C, when the Ni molar ratio increases to over 5 the methanol conversion decreases sharply. The XRD and BET results shows that the Ni particles loaded on the Mo_2C were sintered together and covered the surface of molybdenum carbide at a high Ni/Mo ratio (5/95, 10/90, and 15/85), which results in the decrease in the methanol conversion. The superior catalytic activity of lower Ni/Mo (0.8/99.2–2.4/97.6) is due to the synergistic effect between Ni and native Mo_2C which plays a prominent role in the methanol conversion. Fig. 16b shows the stability of β-Mo_2C, Fe-Mo_2C (1.6), Co-Mo_2C (1.6), and Ni-Mo_2C (1.6) catalysts for the MSR reactions at 400 °C. The Ni-Mo_2C (1.6) showed a comparatively longer catalytic stability and the higher methanol conversion for 12 h. XPS studies show that Mo^{2+} species on fresh and spent β-Mo_2C decreases from 40% to 8% due to surface oxidation. The high performance and stability of Ni modified Mo_2C may be due to a higher resistance to oxidation than pure molybdenum carbide and Fe-, Co modified carbides catalyst.

$LaCoO_3$-based perovskite oxides have also been studied for several oxidation and reduction reactions. Recently, La–Sr–Co–FeO perovskite mixed oxides have attracted considerable attention due to their high mixed electronic-ionic conduction properties and a good catalytic activity towards methane oxidation, as well as their chemical stability in the reducing conditions. Kuc et al. studied the effect of Pd and Zn substation on the $LaCo_{1-x-y}Pd_xZn_yO_{3\pm\delta}$ perovskite catalyst for

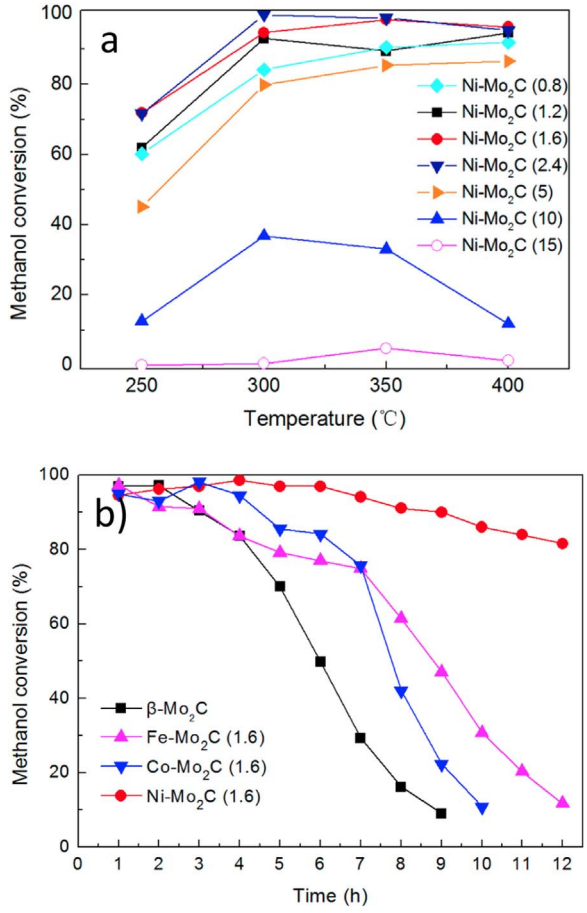

Fig. 16. (a) Catalytic performances of Ni-modified molybdenum carbide with different doping amounts. (b) Stability of β-Mo_2C, Fe-Mo_2C (1.6), Co-Mo_2C (1.6), and Ni-Mo_2C (1.6) catalysts for the SRM reaction at 400 °C [209].

MSR [210]. A series of $LaCoO_{3\pm\delta}$ (LCO), $LaCo_{0.873}Pd_{0.127}O_{3\pm\delta}$ (LCPO), $LaCo_{0.89}Zn_{0.11}O_{3\pm\delta}$ (LCZO), $LaCo_{0.95}Pd_{0.025}Zn_{0.025}O_{3\pm\delta}$ (LCPZO-5), $LaCo_{0.85}Pd_{0.075}Zn_{0.075}O_{3\pm\delta}$ (LCPZO-15), and $LaCo_{0.75}Pd_{0.125}Zn_{0.125}O_{3\pm\delta}$ (LCPZO-25) perovskite oxides were prepared by the Pechini method and calcined at 800 °C in air. The methanol conversion and CO_2 selectivity were studied for all the perovskite compositions. It was observed that Pd and Zn containing LCPZO-5, LCPZO-15 and LCPZO-25 show superior CO_2 selectivity in the 200–400 °C temperature range than the un-substituted or mono substituted materials LCO, LCPO and LCZO. For example, at 225 °C, the CO_2 selectivity is around 11% on un-substituted LCO, on the other hand, for substituted it is between 70% and 91% over Pd and Zn containing perovskite materials. The CO_2 selectivity was shown to improve with increasing Pd and Zn content in LCPZO-5 and LCPZO-15. Fig. 17 shows the 1st derivative of the mass loss curves (DTG) of the perovskite catalyst materials. From Fig. 17b it is evident that the positions of low-temperature DTG curves shifts progressively to lower temperatures with increasing Pd (and Zn) content in the due to the increased reducibility with the presence of the Pd substituent, the materials with both Pd and Zn (LCPZO) leading to significantly improve the MSR activity (≥ 80% CO_2 selectivity).

4.2. Reforming of ethanol for H_2 production

For ethanol steam reforming Rh [211,212] and Ni [213] based catalysts are the most commonly studied with a very high selective towards hydrogen production. The studied supports were Al_2O_3 [214,215], MgO [216,217], ZrO_2 [218], CeO_2 [219], La_2O_3 [220], Nb_2O_5 [219], perovskites [221,222] and bi-metallic [223,224]. A comparative study of ESR on two series of catalysts: (i) Ni deposited on CeO_2 or La_2O_3 promoted alumina; and (ii) Ni deposited on CeO_2 or La_2O_3 promoted zirconia were reported by Dan et al. [225]. The catalysts were prepared through the impregnation method on Al_2O_3 and ZrO_2 supports with an aqueous solution of Ce and La followed by calcining. The mixed supports contain 6 wt% CeO_2 and 6 wt% La_2O_3. Finally Ni (8 wt%) was introduced on the CeO_2-Al_2O_3, La_2O_3-Al_2O_3, CeO_2-ZrO_2, and La_2O_3-ZrO_2 supports, followed by calcination in argon at 550 °C and reduction in H_2 at 550 °C. Fig. 18 shows the catalytic activity of the Ni supported, CeO_2 and La_2O_3 promoted, Al_2O_3, and ZrO_2 catalysts for ESR at temperatures between 150–350 °C. For both the Al_2O_3, and ZrO_2 catalysts promoted with La_2O_3, 100% ethanol conversion was reported at 300 °C. Also, the ESR was improved by addition of CeO_2 on the ZrO_2 supported catalyst, addition of CeO_2 on Al_2O_3 was not significant on the ethanol conversion.

High H_2 yield was observed by coupling the Rh/CeO_2 catalyst on ESR at 400 °C, this was due to the remarkable C–C bond breaking capacity of the Rh catalyst [211]. CeO_2 support was prepared by the urea precipitation process and was then calcined in air at 400 °C. 1% Rh loaded catalyst was further prepared by a deposition-precipitation method. Fig. 19 shows the ESR over the Rh/CeO_2 catalyst. At 400 °C, ethanol and other intermediate products like acetone, acetaldehydes were not detected, suggesting that ethanol was entirely converted into hydrogen and other C_1 products (CO, CO_2, CH_4). At high temperature (650 °C), the reformed gas contains 72 mol% H_2, 14 mol% CO, 10 mol% CO_2 and 4 mol% CH_4.

For the Ni on perovskite supports, Ni/BZCYYb ($BaZr_{0.1}Ce_{0.7}Y_{0.1}Yb_{0.1}O_3$), Ni/BZCY7 ($BaZr_{0.1}Ce_{0.7}Y_{0.2}O_3$) and Ni/BZCY4 ($BaZr_{0.4}Ce_{0.4}Y_{0.2}O_3$) a higher catalytic activity and lower carbon deposition than other oxide catalysts was observed [222,226]. Ex situ Raman spectroscopy was performed to investigate carbon formed on the catalyst (Fig. 20). Without the addition of steam in the feed, Ni/BZCYYb and Ni/BZCY7 display comparable graphitization. When the steam content is increased in the feed, the carbon deposition was much lower in the Ni/BZCYYb catalyst than in the Ni/BZCY7 catalyst. It was reported that the high carbon tolerance of $BaZrO_3$-$BaCeO_3$ oxides is due to the water storage capability, the addition of Yb effectively improves the catalytic activity for the ethanol steam reforming reactions. The stored water in the proton-conducting oxide may react with deposited carbon forming relevant gases thus carbon deposition was alleviated.

5. Poisoning of catalysts for reforming and partial oxidation of hydrocarbons

The stability of catalysts for reforming and partial oxidation of hydrocarbons is extremely important. The deactivation and regeneration of catalysts may be caused by various reasons including chemical, thermal and mechanical which have been reviewed by Argyle et al. [258]. The recent progress beyond this excellent review is briefly described below. Poisoning by impurities, mainly sulphur is the major challenge for reforming and partial oxidation catalysts, whilecoking also poses a problem for reforming catalysts, particularly at low oxygen partial pressure. Recently Ocsachoque et al. reported that the Rh/CeO_2 catalyst exhibits a higher tolerance to sulphur than the Ni/CeO_2 catalyst, this is because of the existence of O^{2-} species in the former. The O^{2-} species can help to oxidize sulphur into SO_x [259]. As for the conventional Ni/Al_2O_3 catalyst, it was found that a high sintering temperature is beneficial to the anti-coking property when performing the CO_2 reforming of methane. $NiAl_2O_4$ will be formed at high temperature while Ni particles formed from the reduction of $NiAl_2O_4$ have a strong interaction with the support while carbon deposition did not affect the contact of gases with the supported Ni catalysts thus the activity remains [260]. Not only methane, reforming of dodecane and liquefied petroleum gas has attracted the attention of researchers. It was found that $LaNiO_3$ nanocrystals in SBA-15 mesoporous SiO_2 exhibits high stability and anti-coking on steam reforming of liquefied petroleum [261].

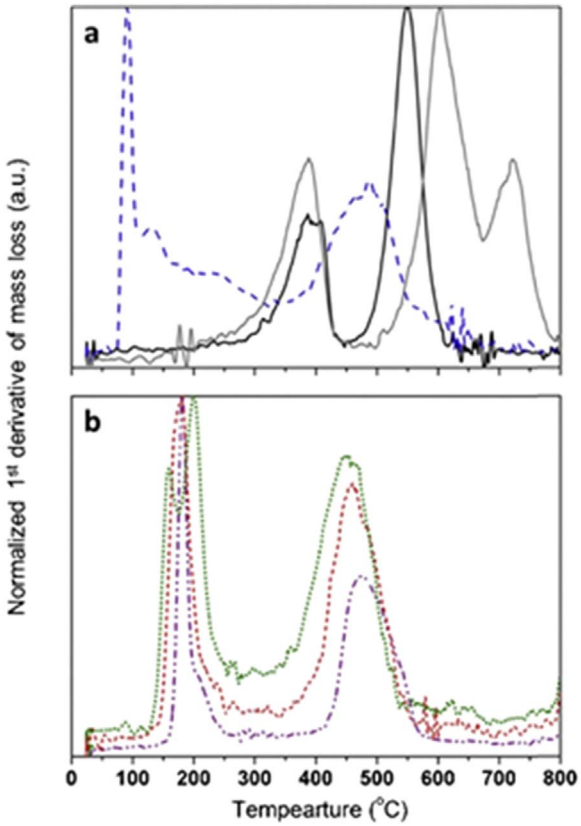

Fig. 17. 1st derivative of the mass loss (DTG) curves of (a) LCO (——), LCPO (— — —) and LCZO (——) and (b) LCPZO-5 (— · — · —), LCPZO-15 (— — — —) and LCPZO-25 (· · · · · ·) [210].

6. Reforming and partial oxidation catalysts for direct hydrocarbon solid oxide fuel cells

The high fuel flexibility offered by SOFCs gives the possibility to use relatively cheap, safe, and readily available hydrocarbons. However more direct utilization of such fuels would greatly lower fuel cost and increase the feasibility of SOFC commercialization, especially for near-term adoption in high value markets. This also allows the technology to create a bridge towards the anticipated arrival of the "hydrogen economy". Current SOFC technology has shown good performance with a wide range of hydrocarbon and syngas fuels, but there are still significant challenges for practical application [262]. The direct utilization of hydrocarbons in an SOFC was reported by Vohs et al. as early as 1995 but the power density was not high [263]. In 1999, Barnett et al. reported a direct methane SOFC without carbon deposition when a 0.5 μm thick $(Y_2O_3)_{0.15}(CeO_2)_{0.85}$(YDC) porous film was used between the Ni-Y_2O_3-stabilized ZrO_2 (YSZ) anode and YSZ electrolyte [264]. In 2000, Gorte et al. extended the hydrocarbon fuels for SOFCs from methane to ethane, 1-butene, n-butane and toluene [265]. The development of anodes for hydrocarbon SOFCs have been reviewed in several papers [61,262,266,267]. Reformed liquid hydrocarbons such as n-dodecane and diesel are also reported as fuels for SOFCs with good performance although the degradation is slightly higher than that when H_2 was used as the fuel [268–270]. MoO_2 has been identified as a conductive anti-coking anode running on reformed diesel. There is also some initial work on the reforming of diesel/biodiesel to be used as fuels for SOFCs [271].

Conventional Ni-based anodes for SOFCs suffer from carbon deposition due to Ni being an excellent hydrocarbon decomposition catalyst. While this can be avoided to a large extent by having excess water in the system to promote steam reforming reactions, this requirement can increase system complexity and add water management issues. The ability to utilise the fuel directly with less or no additional water would be a great benefit for system by reducing the cost, thus a good reforming catalyst that can work at low steam to carbon ratios would be ideal. This can be realised whether as part of direct utilization on the anode itself or as part of a robust pre-reforming catalyst supplying partly reformed fuel to the anode. It has been reported that when Ni is replaced by Cu, Cu alloys, or with the integration of CeO_2, carbon deposition can be alleviated [265,272]. Liu reported that BaO-Ni/YSZ anode can run C_3H_8 as the fuel exhibiting stable performance for 100 h [59]. The first redox perovskite-based anode $(La_{0.75}Sr_{0.25})Cr_{0.5}Mn_{0.5}O_{3-\delta}$ (LSCM) was discovered by Tao and Irvine. This can run on methane as the fuel with negligible carbon deposition [4]. Other material families such as titanate [273], vanadate [61,274] and double perovskite [275] are also reported to be redox stable/reversible and with promising performances when run on hydrocarbon fuels [61,267]. Besides these requirements, carbon deposition, tolerance to impurities (particularly sulphur), long term operational reliability and durability remain challenges, especially when liquid hydrocarbons such as diesel/bio-diesel are used as the fuel. Therefore some element of pre-reforming is essential in these cases [262]. For gaseous hydrocarbons, reforming of the fuels will generate H_2 and CO to be used as the fuels for SOFCs however, care must still be exercised to prevent reverse water gas shift reactions resulting in the formation of solid carbon. Anti-coking can also be achieved through tailoring of microstructure. It has been reported that hierarchically porous Ni-based anode deposited with a nanocatalyst layer has improved coking resistance when methane was used as the fuel. A thin layer of nano samaria doped ceria catalyst was infiltrated on the walls of Ni-yttria-stabilised zirconia anode. The cell efficiency has been improved with a power density of 650 mW cm^{-2} at 800 °C when methane was used as the fuel while the performance is stable for over 400 h. This study provides an excellent strategy in developing anti-coking anodes for SOFCs [276]. In addition to carbon deposition and poisoning, sintering of catalysts is a further key challenge in order to realise a stable robust anode for SOFCs. In general, oxidation of hydrogen is easier than that for CO and hydrocarbons. An anode with integrated reforming or oxidation catalysts for in situ hydrogen

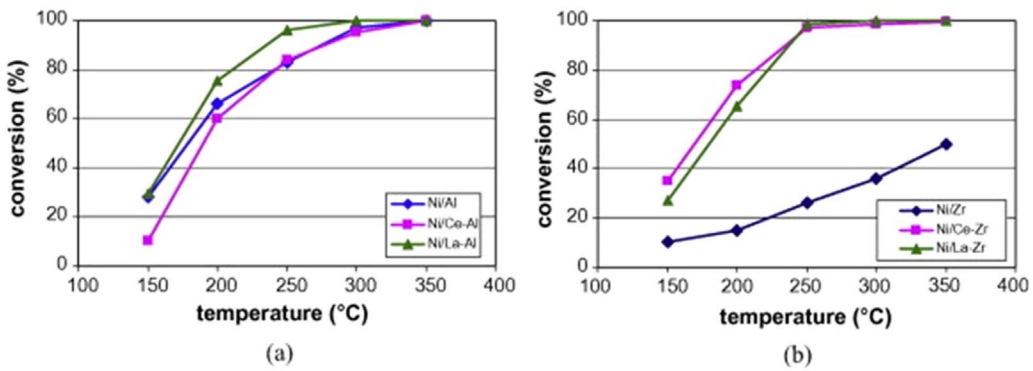

Fig. 18. The variation of ethanol conversion with temperature in ethanol steam reforming reactions catalyzed by: (a) alumina supported Ni catalysts and (b) zirconia supported Ni catalysts; 1 g catalyst, 0.1 ml/min liquid flow, 35 ml/min Ar flow [225].

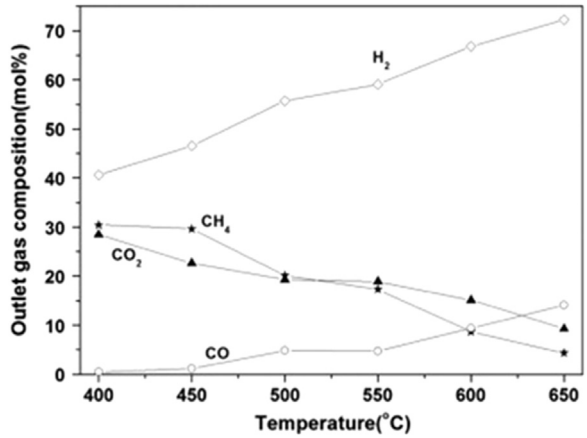

Fig. 19. Effect of reaction temperature on the product distribution of ethanol steam reforming over the Rh/CeO_2 catalyst. C_2H_5OH/H_2O = 1/3, molar ratio; GHSV: 6000 h^{-1} [211].

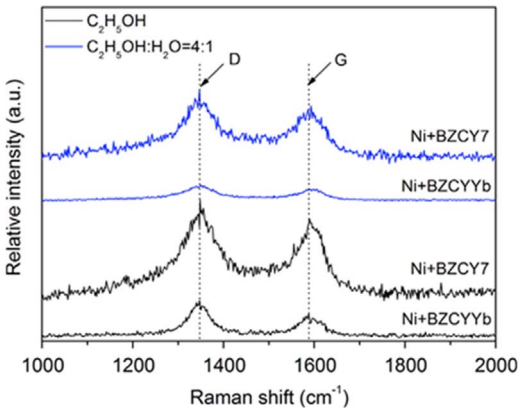

Fig. 20. Raman spectra of the deposited carbon on the Ni/BZCYYb and Ni/BZCY7 catalyst after treatment in ethanol-containing atmospheres for 30 min at 600 °C [222].

production at the anode may facilitate the fuel oxidation thus reduce anode polarization resistance resulting in enhanced performance [60].

7. Challenges and future work

Although the focus of this review is on the catalytic activity, the development of hydrocarbon reforming for hydrogen or hydrogen rich syngas generation for fuel cells has been the focus of a remarkable quantity of research efforts in order to understand factors such as the reforming catalyst structure, the reforming reaction and fuel processing. These areas are also important but are not within the scope of this paper. Tolerance to impurities such as sulphur and anti-coking are important for fuel cells which are also highlighted. By performing a comparative literature study it can be seen that the most common preparation method for the reforming catalyst is the wet impregnation technique. By using the proper preparation method and appropriate catalyst support then it is possible to maximize the key catalyst parameters such as hydrocarbon conversion, hydrogen production and selectivity. Key catalyst parameters including hydrogen selectivity, thermal stability, chemical stability and carbon deposition tolerance can be improved by the addition of catalyst promoters as well as the choice of catalyst support. The catalyst promoters are usually in the form of other metals which are added to the Ni catalyst thereby forming an M-Ni bi-metallic alloy catalyst. From the literature it can be found that the good performing catalyst promoters are Co, Cu, Sn, Pt, Pd, Mn, Rh, Ru and Au which have been reported to greatly improve the hydrogen production of the Ni catalyst while also decreasing carbon deposition. To conclude, the growth in the exploration in the design and identification of new reforming catalysts has led to the development of new effective catalyst with improved performance for hydrocarbon reforming for hydrogen or hydrogen rich gas generation for fuel cells. To avoid or simplify the gas separation process, sorption – enhancement and chemical looping steam reforming of hydrocarbons, particularly methane is promising. However, the cyclability of the CO_2 sorbent, the oxygen carrier catalyst, anti-coking and slow kinetics etc are all major challenges. It is desired to develop new catalysts with low cost, that are both chemically and mechanically stable (keep microstructure, negligible sintering/coarsening at high temperature), tolerant to impurities, anti-coking with high catalytic activities towards reforming and partial oxidation of hydrocarbons for hydrogen production and fuel cell applications.

Acknowledgements

The authors thank EPSRC SuperGen XIV 'Delivery of Sustainable Hydrogen' Project (Grant No EP/G01244X/1), Flame SOFCs (EP/K021036/2), UK-India Biogas SOFCs (EP/I037016/1) and SuperGen Fuel Cells (EP/G030995/1) projects for funding.

References

[1] Jacobson AJ. Materials for solid oxide fuel cells. Chem Mater 2010;22:660–74.
[2] Shao Z, Haile SM. A high-performance cathode for the next generation of solid-oxide fuel cells. Nature 2004;431:170–3.
[3] Park S, Vohs JM, Gorte RJ. Direct oxidation of hydrocarbons in a solid-oxide fuel cell. Nature 2000;404:265–7.
[4] Tao SW, Irvine JTS. A redox-stable efficient anode for solid-oxide fuel cells. Nat Mater 2003;2:320–3.
[5] Steele BCH, Heinzel A. Materials for fuel-cell technologies. Nature 2001;414:345–52.
[6] Brett DJL, Atkinson A, Brandon NP, Skinner SJ. Intermediate temperature solid oxide fuel cells. Chem Soc Rev 2008;37:1568–78.
[7] Wachsman ED, Lee KT. Lowering the temperature of solid oxide fuel cells. Science 2011;334:935–9.
[8] Atkinson A, Barnett S, Gorte RJ, Irvine JTS, McEvoy AJ, Mogensen M, et al. Advanced anodes for high-temperature fuel cells. Nat Mater 2004;3:17–27.
[9] Minh NQ. Solid oxide fuel cell technology—features and applications. Solid State Ion 2004;174:271–7.
[10] Tao SW, Irvine JTS, Plint SM. Methane oxidation at redox stable fuel cell electrode $La_{0.75}Sr_{0.25}Cr_{0.5}Mn_{0.5}O_{3-\delta}$. J Phys Chem B 2006;110:21771–6.
[11] Tao SW, Irvine JTS. Catalytic properties of the perovskite oxide $La_{0.75}Sr_{0.25}Cr_{0.5}Fe_{0.5}O_{3-\delta}$ in relation to its potential as a solid oxide fuel cell anode material. Chem Mater 2004;16:4116–21.
[12] Sengodan S, Choi S, Jun A, Shin TH, Ju Y-W, Jeong HY, et al. Layered oxygen-deficient double perovskite as an efficient and stable anode for direct hydrocarbon solid oxide fuel cells. Nat Mater 2015;14:205–9.
[13] Sengodan S, Liu M, Lim T-H, Shin J, Liu M, Kim G. Enhancing sulfur tolerance of a Ni-YSZ anode through $BaZr_{0.1}Ce_{0.7}Y_{0.1}Yb_{0.1}O_{3-\delta}$ infiltration. J Electrochem Soc 2014;161:F668–73.
[14] Sengodan S, Yeo HJ, Shin JY, Kim G. Assessment of perovskite-type $La_{0.8}Sr_{0.2}Sc_xMn_{1-x}O_{3-\delta}$ oxides as anodes for intermediate-temperature solid oxide fuel cells using hydrocarbon fuels. J Power Sources 2011;196:3083–8.
[15] Vohs JM, Gorte RJ. High-performance SOFC cathodes prepared by infiltration. Adv Mater 2009;21:943–56.
[16] Goodenough JB, Huang Y-H. Alternative anode materials for solid oxide fuel cells. J Power Sources 2007;173:1–10.
[17] Gorte RJ, Vohs JM. Nanostructured anodes for solid oxide fuel cells. Curr Opin Colloid Interface Sci 2009;14:236–44.
[18] Murray EP, Tsai T, Barnett SA. A direct-methane fuel cell with a ceria-based anode. Nature 1999;400:649–51.
[19] Zhan Z, Barnett SA. An octane-fueled solid oxide fuel cell. Science 2005;308:844–7.
[20] Liu M, Choi Y, Yang L, Blinn K, Qin W, Liu P, et al. Direct octane fuel cells: a promising power for transportation. Nano Energy 2012;1:448–55.
[21] McIntosh S, Gorte RJ. Direct hydrocarbon solid oxide fuel cells. Chem Rev 2004;104:4845–66.
[22] Yang L, Choi Y, Qin W, Chen H, Blinn K, Liu M, et al. Promotion of water-mediated carbon removal by nanostructured barium oxide/nickel interfaces in solid oxide fuel cells. Nat Commun 2011;2:357.
[23] Andersson M, Paradis H, Yuan J, Sundén B. Review of catalyst materials and catalytic steam reforming reactions in SOFC anodes. Int J Energy Res 2011;35:1340–50.
[24] Angeli SD, Monteleone G, Giaconia A, Lemonidou AA. State-of-the-art catalysts for CH4 steam reforming at low temperature. Int J Hydrog Energy 2014;39:1979–97.
[25] Ashcroft AT, Cheetham AK, Foord JS, Green MLH, Grey CP, Murrell AJ, et al. Selective oxidation of methane to synthesis gas using transition metal catalysts. Nature 1990;344:319–21.

[26] Ashcroft AT, Cheetham AK, Green MLH, Vernon PDF. Partial oxidation of methane to synthesis gas using carbon dioxide. Nature 1991;352:225–6.
[27] Cheekatamarla PK, Finnerty CM. Reforming catalysts for hydrogen generation in fuel cell applications. J Power Sources 2006;160:490–9.
[28] Clarke SH, Dicks AL, Pointon K, Smith TA, Swann A. Catalytic aspects of the steam reforming of hydrocarbons in internal reforming fuel cells. Catal Today 1997;38:411–23.
[29] Holladay JD, Hu J, King DL, Wang Y. An overview of hydrogen production technologies. Catal Today 2009;139:244–60.
[30] Wei Z, Sun J, Li Y, Datye AK, Wang Y. Bimetallic catalysts for hydrogen generation. Chem Soc Rev 2012;41:7994–8008.
[31] Xuan J, Leung MKH, Leung DYC, Ni M. A review of biomass-derived fuel processors for fuel cell systems. Renew Sustain Energy Rev 2009;13:1301–13.
[32] Arcotumapathy V, Vo D-VN, Chesterfield D, Tin CT, Siahvashi A, Lucien FP, et al. Catalyst design for methane steam reforming. Appl Catal A: Gen 2014;479:87–102.
[33] Contreras JL, Salmones J, Colín-Luna JA, Nuño L, Quintana B, Córdova I, et al. Catalysts for H_2 production using the ethanol steam reforming (a review). Int J Hydrog Energy 2014;39:18835–53.
[34] Sá S, Silva H, Brandão L, Sousa JM, Mendes A. Catalysts for methanol steam reforming—a review. Appl Catal B: Environ 2010;99:43–57.
[35] Ghenciu AF. Review of fuel processing catalysts for hydrogen production in PEM fuel cell systems. Curr Opin Solid State Mater Sci 2002;6:389–99.
[36] Pakhare D, Spivey J. A review of dry (CO_2) reforming of methane over noble metal catalysts. Chem Soc Rev 2014;43:7813–37.
[37] Enger BC, Lodeng R, Holmen A. A review of catalytic partial oxidation of methane to synthesis gas with emphasis on reaction mechanisms over transition metal catalysts. Appl Catal A-Gen 2008;346:1–27.
[38] Adhikari S, Fernando SD, Haryanto A. Hydrogen production from glycerol: an update. Energy Convers Manag 2009;50:2600–4.
[39] Haryanto A, Fernando S, Murali N, Adhikari S. Current status of hydrogen production techniques by steam reforming of ethanol: a review. Energy Fuels 2005;19:2098–106.
[40] Hecht ES, Gupta GK, Zhu H, Dean AM, Kee RJ, Maier L, et al. Methane reforming kinetics within a Ni–YSZ SOFC anode support. Appl Catal A: Gen 2005;295:40–51.
[41] Huang B, Wang SR, Liu RZ, Wen TL. Preparation and performance characterization of the Fe–Ni/ScSZ cermet anode for oxidation of ethanol fuel in SOFCs. J Power Sources 2007;167:288–94.
[42] Douvartzides SL, Coutelieris FA, Demin AK, Tsiakaras PE. Electricity from ethanol fed SOFCs: the expectations for sustainable development and technological benefits. Int J Hydrog Energy 2004;29:375–9.
[43] Liese EA, Gemmen RS. Performance comparison of internal reforming against external reforming in a solid oxide fuel cell, gas turbine hybrid system. J Eng Gas Turbines Power 2005;127:86–90.
[44] Sun C, Stimming U. Recent anode advances in solid oxide fuel cells. J Power Sources 2007;171:247–60.
[45] Sun C, Xie Z, Xia C, Li H, Chen L. Investigations of mesoporous CeO_2–Ru as a reforming catalyst layer for solid oxide fuel cells. Electrochem Commun 2006;8:833–8.
[46] Klein J-M, Hénault M, Roux C, Bultel Y, Georges S. Direct methane solid oxide fuel cell working by gradual internal steam reforming: analysis of operation. J Power Sources 2009;193:331–7.
[47] Klein J-M, Hénault M, Gélin P, Bultel Y, Georges S. A solid oxide fuel cell operating in gradual internal reforming conditions under pure dry methane. Electrochem Solid-State Lett 2008;11:B144–7.
[48] Wang W, Ran R, Shao Z. Combustion-synthesized Ru–Al_2O_3 composites as anode catalyst layer of a solid oxide fuel cell operating on methane. Int J Hydrog Energy 2011;36:755–64.
[49] Wang W, Ran R, Shao Z. Lithium and lanthanum promoted Ni-Al_2O_3 as an active and highly coking resistant catalyst layer for solid-oxide fuel cells operating on methane. J Power Sources 2011;196:90–7.
[50] Wang W, Su C, Ran R, Shao Z. A new Gd-promoted nickel catalyst for methane conversion to syngas and as an anode functional layer in a solid oxide fuel cell. J Power Sources 2011;196:3855–62.
[51] Wang W, Su C, Ran R, Park HJ, Kwak C, Shao Z. Physically mixed LiLaNi–Al_2O_3 and copper as conductive anode catalysts in a solid oxide fuel cell for methane internal reforming and partial oxidation. Int J Hydrog Energy 2011;36:5632–43.
[52] Lee SH, Kim H. Dual layered anode support for the internal reforming of methane for solid oxide fuel cells. Ceram Int 2014;40:5959–66.
[53] Liao M, Wang W, Ran R, Shao Z. Development of a Ni–$Ce_{0.8}Zr_{0.2}O_2$ catalyst for solid oxide fuel cells operating on ethanol through internal reforming. J Power Sources 2011;196:6177–85.
[54] Ye X-F, Huang B, Wang SR, Wang ZR, Xiong L, Wen TL. Preparation and performance of a Cu–CeO_2–ScSZ composite anode for SOFCs running on ethanol fuel. J Power Sources 2007;164:203–9.
[55] Azimova MA, McIntosh S. Properties and Performance of anode-supported proton-conducting $BaCe_{0.48}Zr_{0.4}Yb_{0.1}Co_{0.02}O_{3-\delta}$ solid oxide fuel cells. J Electrochem Soc 2010;157:B1397–402.
[56] Duan C, Tong J, Shang M, Nikodemski S, Sanders M, Ricote S, et al. Readily processed protonic ceramic fuel cells with high performance at low temperatures. Science 2015;349:1321–6.
[57] Jin C, Yang C, Zhao F, Coffin A, Chen F. Direct-methane solid oxide fuel cells with $Cu_{1.3}Mn_{1.7}O_4$ spinel internal reforming layer. Electrochem Commun 2010;12:1450–2.
[58] Jin C, Yang C, Zheng H, Chen F. Intermediate temperature solid oxide fuel cells with $Cu_{1.3}Mn_{1.7}O_4$ internal reforming layer. J Power Sources 2012;201:66–71.
[59] Yang L, Choi Y, Qin W, Chen H, Blinn K, Liu M, et al. Promotion of water-mediated carbon removal by nanostructured barium oxide/nickel interfaces in solid oxide fuel cells. Nat Commun 2011;2.
[60] Cowin PI, Petit CTG, Lan R, Irvine JTS, Tao SW. Recent progress in the development of anode materials for solid oxide fuel cells. Adv Energy Mater 2011;1:314–32.
[61] Ge X-M, Chan S-H, Liu Q-L, Sun Q. Solid oxide fuel cell anode materials for direct hydrocarbon utilization. Adv Energy Mater 2012;2:1156–81.
[62] Zhang Y, Wang W, Wang Z, Zhou X, Wang Z, Liu C-J. Steam reforming of methane over Ni/SiO_2 catalyst with enhanced coke resistance at low steam to methane ratio. Catal Today 2015;256:130–6.
[63] Wang Z, Shao X, Hu X, Parkinson G, Xie K, Dong D, et al. Hierarchically structured NiO/CeO_2 nanocatalysts templated by eggshell membranes for methane steam reforming. Catal Today 2014;228:199–205.
[64] Ma Y, Wang X, You X, Liu J, Tian J, Xu X, et al. Nickel-supported on $La_2Sn_2O_7$ and $La_2Zr_2O_7$ pyrochlores for methane steam reforming: insight into the difference between tin and zirconium in the B site of the compound. ChemCatChem 2014;6:3366–76.
[65] Xue X, Wu S. The microstructure and stability of a Ni-nano-CaO/Al_2O_3 reforming catalyst under carbonation–calcination cycling conditions. Int J Hydrog Energy 2015;40:5617–23.
[66] Kim TW, Park JC, Lim T-H, Jung H, Chun DH, Lee HT, et al. The kinetics of steam methane reforming over a Ni/γ-Al_2O_3 catalyst for the development of small stationary reformers. Int J Hydrog Energy 2015;40:4512–8.
[67] Zhou L, Guo Y, Kameyama H, Basset J-M. An anodic alumina supported Ni–Pt bimetallic plate-type catalysts for multi-reforming of methane, kerosene and ethanol. Int J Hydrog Energy 2014;39:7291–305.
[68] Özkara-Aydınoğlu Ş, Aksoylu AE. CO_2 reforming of methane over Pt–Ni/Al_2O_3 catalysts: effects of catalyst composition, and water and oxygen addition to the feed. Int J Hydrog Energy 2011;36:2950–9.
[69] Foletto EL, Alves RW, Jahn SL. Preparation of Ni/Pt catalysts supported on spinel ($MgAl_2O_4$) for methane reforming. J Power Sources 2006;161:531–4.
[70] Khzouz M, Wood J, Pollet B, Bujalski W. Characterization and activity test of commercial Ni/Al_2O_3, Cu/ZnO/Al_2O_3 and prepared Ni–Cu/Al_2O_3 catalysts for hydrogen production from methane and methanol fuels. Int J Hydrog Energy 2013;38:1664–75.
[71] Luna EC, Becerra AM, Dimitrijewits MI. Methane steam reforming over rhodium promoted Ni/Al_2O_3 catalysts. React Kinet Catal Lett 1999;67:247–52.
[72] Dan M, Mihet M, Biris A, Marginean P, Almasan V, Borodi G, et al. Supported nickel catalysts for low temperature methane steam reforming: comparison between metal additives and support modification. React Kinet Mech Catal 2012;105:173–93.
[73] Maluf SS, Assaf EM. Ni catalysts with Mo promoter for methane steam reforming. Fuel 2009;88:1547–53.
[74] Parizotto NV, Rocha KO, Damyanova S, Passos FB, Zanchet D, Marques CMP, et al. Alumina-supported Ni catalysts modified with silver for the steam reforming of methane: effect of Ag on the control of coke formation. Appl Catal A: Gen 2007;330:12–22.
[75] Majewski AJ, Wood J, Bujalski W. Nickel–silica core@shell catalyst for methane reforming. Int J Hydrog Energy 2013;38:14531–41.
[76] Li Z, Devianto H, Kwon H-H, Yoon SP, Lim T-H, Lee H-I. The catalytic performance of Ni/$MgSiO_3$ catalyst for methane steam reforming in operation of direct internal reforming MCFC. J Ind Eng Chem 2010;16:485–9.
[77] Miyata T, Li D, Shiraga M, Shishido T, Oumi Y, Sano T, et al. Promoting effect of Rh, Pd and Pt noble metals to the Ni/Mg(Al)O catalysts for the DSS-like operation in CH4 steam reforming. Appl Catal A: Gen 2006;310:97–104.
[78] Kusakabe K, Sotowa K-I, Eda T, Iwamoto Y. Methane steam reforming over Ce–ZrO_2-supported noble metal catalysts at low temperature. Fuel Process Technol 2004;86:319–26.
[79] Andrade ML, Almeida L, do Carmo Rangel M, Pompeo F, Nichio N. Ni-catalysts supported on Gd-doped ceria for solid oxide fuel cells in methane steam reforming. Chem Eng Technol 2014;37:343–8.
[80] Harshini D, Lee DH, Jeong J, Kim Y, Nam SW, Ham HC, et al. Enhanced oxygen storage capacity of $Ce_{0.65}Hf_{0.25}M_{0.1}O_{2-\delta}$ (M = rare earth elements): applications to methane steam reforming with high coking resistance. Appl Catal B: Environ 2014;148–149:415–23.
[81] Lertwittayanon K, Atong D, Aungkavattana P, Wasanapiarnpong T, Wada S, Sricharoenchaikul V. Effect of CaO–ZrO_2 addition to Ni supported on γ-Al_2O_3 by sequential impregnation in steam methane reforming. Int J Hydrog Energy 2010;35:12277–85.
[82] Nawfal M, Gennequin C, Labaki M, Nsouli B, Aboukaïs A, Abi-Aad E. Hydrogen production by methane steam reforming over Ru supported on Ni–Mg–Al mixed oxides prepared via hydrotalcite route. Int J Hydrog Energy 2015;40:1269–77.
[83] Homsi D, Aouad S, Gennequin C, Aboukaïs A, Abi-Aad E. A highly reactive and stable Ru/$Co_{6-x}Mg_xAl_2$ catalyst for hydrogen production via methane steam reforming. Int J Hydrog Energy 2014;39:10101–7.
[84] U-e-s Amjad, Gonçalves Lenzi G, Camargo Fernandes-Machado NR, Specchia S. MgO and N_b2_O5 oxides used as supports for Ru-based catalysts for the methane steam reforming reaction. Catal Today 2015;257, Part 1:122–30.
[85] Vita A, Cristiano G, Italiano C, Pino L, Specchia S. Syngas production by methane oxy-steam reforming on Me/CeO_2 (Me = Rh, Pt, Ni) catalyst lined on cordierite monoliths. Appl Catal B: Environ 2015;162:551–63.
[86] Duarte RB, Nachtegaal M, Bueno JMC, van Bokhoven JA. Understanding the effect of Sm_2O_3 and CeO_2 promoters on the structure and activity of Rh/Al_2O_3 catalysts in methane steam reforming. J Catal 2012;296:86–98.
[87] Shinde VM, Madras G. Production of syngas from steam reforming and CO removal with water gas shift reaction over nanosized $Zr_{0.95}Ru_{0.05}O_{2-\delta}$ solid solution. Int J

Hydrog Energy 2013;38:13961–73.
[88] Pereñíguez R, González-DelaCruz VM, Holgado JP, Caballero A. Synthesis and characterization of a $LaNiO_3$ perovskite as precursor for methane reforming reactions catalysts. Appl Catal B: Environ 2010;93:346–53.
[89] Simakov DSA, Luo HY, Román-Leshkov Y. Ultra-low loading Ru/γ-Al_2O_3: a highly active and stable catalyst for low temperature solar thermal reforming of methane. Appl Catal B: Environ 2015;168–169:540–9.
[90] Roy PS, Park N-K, Kim K. Metal foam-supported Pd–Rh catalyst for steam methane reforming and its application to SOFC fuel processing. Int J Hydrog Energy 2014;39:4299–310.
[91] Cassinelli WH, Damyanova S, Parizotto NV, Zanchet D, Bueno JMC, Marques CMP. Study of the properties of supported Pd catalysts for steam and autothermal reforming of methane. Appl Catal A: Gen 2014;475:256–69.
[92] Rocha KO, Santos JBO, Meira D, Pizani PS, Marques CMP, Zanchet D, et al. Catalytic partial oxidation and steam reforming of methane on La_2O_3–Al_2O_3 supported Pt catalysts as observed by X-ray absorption spectroscopy. Appl Catal A: Gen 2012;431–432:79–87.
[93] Yu M, Zhu Y-A, Lu Y, Tong G, Zhu K, Zhou X. The promoting role of Ag in Ni-CeO_2 catalyzed CH_4-CO_2 dry reforming reaction. Appl Catal B: Environ 2015;165:43–56.
[94] Nikolla E, Schwank J, Linic S. Promotion of the long-term stability of reforming Ni catalysts by surface alloying. J Catal 2007;250:85–93.
[95] Nikolla E, Schwank J, Linic S. Comparative study of the kinetics of methane steam reforming on supported Ni and Sn/Ni alloy catalysts: the impact of the formation of Ni alloy on chemistry. J Catal 2009;263:220–7.
[96] Saadi S, Hinnemann B, Helveg S, Appel CC, Abild-Pedersen F, Nørskov JK. First-principles investigations of the Ni3Sn alloy at steam reforming conditions. Surf Sci 2009;603:762–70.
[97] Amjad U-e-s, Gonçalves Lenzi G, Camargo Fernandes-Machado NR, Specchia S. MgO and Nb_2O_5 oxides used as supports for Ru-based catalysts for the methane steam reforming reaction. Catal Today.
[98] Choi SO, Moon SH. Performance of $La_{1-x}Ce_xFe_{0.7}Ni_{0.3}O_3$ perovskite catalysts for methane steam reforming. Catal Today 2009;146:148–53.
[99] Urasaki K, Sekine Y, Kawabe S, Kikuchi E, Matsukata M. Catalytic activities and coking resistance of Ni/perovskites in steam reforming of methane. Appl Catal A: Gen 2005;286:23–9.
[100] Barelli L, Bidini G, Gallorini F, Servili S. Hydrogen production through sorption-enhanced steam methane reforming and membrane technology: a review. Energy 2008;33:554–70.
[101] Harrison DP. Sorption-enhanced hydrogen production: a review. Ind Eng Chem Res 2008;47:6486–501.
[102] Lee KB, Beaver MG, Caram HS, Sircar S. Production of fuel-cell grade hydrogen by thermal swing sorption enhanced reaction concept. Int J Hydrog Energy 2008;33:781–90.
[103] Chao Z, Wang Y, Jakobsen JP, Fernandino M, Jakobsen HA. Numerical investigation of the sorption enhanced steam methane reforming in a fluidized bed reactor. In: Barrio M, Venvik HJ, editors. Proceedings of the 2nd Trondheim gas technology conference; 2012; p. 15–21.
[104] Chen H, Liu J, Guo Z. Kinetics analysis and process simulation for sorption-enhanced steam methane reforming. In: Liu Z, Peng F, Liu X, editors. Advances in chemical engineering II, Pts 1-42012; p. 2633–7.
[105] Dou B, Wang C, Song Y, Chen H, Jiang B, Yang M, et al. Solid sorbents for in-situ CO_2 removal during sorption-enhanced steam reforming process: a review. Renew Sustain Energy Rev 2016;53:536–46.
[106] Steinfeld A, Kuhn P, Karni J. High-temperature solar thermochemistry - production of iron and synthesis gas by Fe3o4-reduction with methane. Energy 1993;18:239–49.
[107] Zhu X, Wei Y, Wang H, Li K. Ce-Fe oxygen carriers for chemical-looping steam methane reforming. Int J Hydrog Energy 2013;38:4492–501.
[108] Tang M, Xu L, Fan M. Progress in oxygen carrier development of methane-based chemical-looping reforming: a review. Appl Energy 2015;151:143–56.
[109] He F, Wei Y, Li H, Wang H. Synthesis gas generation by chemical-looping reforming using Ce-based oxygen carriers modified with Fe, Cu, and Mn oxides. Energy Fuels 2009;23:2095–102.
[110] Zhu X, Li K, Wei Y, Wang H, Sun L. Chemical-looping steam methane reforming over a CeO_2-Fe_2O_3 oxygen carrier: evolution of its structure and reducibility. Energy Fuels 2014;28:754–60.
[111] Zhao K, He F, Huang Z, Wei GQ, Zheng AQ, Li HB, et al. Perovskite-type oxides $LaFe_{1-x}Co_xO_3$ for chemical looping steam methane reforming to syngas and hydrogen co-production. Appl Energy 2016;168:193–203.
[112] Zheng YN, Li KZ, Wang H, Zhu X, Wei YG, Zheng M, et al. Enhanced activity of CeO_2-ZrO_2 solid solutions for chemical-looping reforming of methane via tuning the macroporous structure. Energy Fuels 2016;30:638–47.
[113] Chaubey R, Sahu S, James OO, Maity S. A review on development of industrial processes and emerging techniques for production of hydrogen from renewable and sustainable sources. Renew Sustain Energy Rev 2013;23:443–62.
[114] Meng B, Zhang H, Zhao Z, Wang X, Jin Y, Liu S. A novel $LaGa_{0.65}Mg_{0.15}Ni_{0.20}O_{3-\delta}$ perovskite catalyst with high performance for the partial oxidation of methane to syngas. Catal Today.
[115] Basile F, Fornasari G, Trifirò F, Vaccari A. Rh–Ni synergy in the catalytic partial oxidation of methane: surface phenomena and catalyst stability. Catal Today 2002;77:215–23.
[116] Parizotto NV, Zanchet D, Rocha KO, Marques CMP, Bueno JMC. The effects of Pt promotion on the oxi-reduction properties of alumina supported nickel catalysts for oxidative steam-reforming of methane: temperature-resolved XAFS analysis. Appl Catal A: Gen 2009;366:122–9.
[117] Enger B, Lødeng R, Holmen A. Effects of noble metal promoters on in situ reduced low loading Ni catalysts for methane activation. Catal Lett 2010;134:13–23.
[118] Ji Y, Li W, Xu H, Chen Y. A study on the ignition process for the catalytic partial oxidation of methane to synthesis gas by MS-TPSR technique. Catal Lett 2001;71:45–8.
[119] Choudhary VR, Prabhakar B, Rajput AM. Beneficial effects of noble metal addition to Ni/Al_2O_3 catalyst for oxidative methane-to-syngas conversion. J Catal 1995;157:752–4.
[120] Wang HY, Ruckenstein E. Conversions of methane to synthesis gas over Co/γ-Al_2O_3 by CO_2 and/or O2. Catal Lett 2001;75:13–8.
[121] Tang S, Lin J, Tan KL. Partial oxidation of methane to synthesis gas over α-Al_2O_3-supported bimetallic Pt–Co catalysts. Catal Lett 1999;59:129–35.
[122] Yang S, Kondo JN, Hayashi K, Hirano M, Domen K, Hosono H. Partial oxidation of methane to syngas over promoted C12A7. Appl Catal A: Gen 2004;277:239–46.
[123] Koh ACW, Chen L, Kee Leong W, Johnson BFG, Khimyak T, Lin J. Hydrogen or synthesis gas production via the partial oxidation of methane over supported nickel–cobalt catalysts. Int J Hydrog Energy 2007;32:725–30.
[124] Wang HY, Ruckenstein E. Partial oxidation of methane to synthesis gas over alkaline earth metal oxide supported cobalt catalysts. J Catal 2001;199:309–17.
[125] Bi X-j, Hong P-j, Xie X-g, Dai S-s. Microwave effect on partial oxidation of methane to syngas. React Kinet Catal Lett 1999;66:381–6.
[126] Choudhary VR, Mondal KC, Choudhary TV. Partial oxidation of methane to syngas with or without simultaneous steam or CO_2 reforming over a high-temperature stable-NiCoMgCeO$_x$ supported on zirconia–hafnia catalyst. Appl Catal A: Gen 2006;306:45–50.
[127] Choudhary VR, Mondal KC, Choudhary TV. Oxy-methane reforming over high temperature stable NiCoMgCeOx and NiCoMgOx supported on zirconia–haffnia catalysts: accelerated sulfur deactivation and regeneration. Catal Commun 2007;8:561–4.
[128] Pudukudy M, Yaakob Z, Akmal ZS. Direct decomposition of methane over SBA-15 supported Ni, Co and Fe based bimetallic catalysts. Appl Surf Sci 2015;330:418–30.
[129] Miao Q, Xiong G, Sheng S, Cui W, Xu L, Guo X. Partial oxidation of methane to syngas over nickel-based catalysts modified by alkali metal oxide and rare earth metal oxide. Appl Catal A: Gen 1997;154:17–27.
[130] Wang H-t, Li Z-h, Tian S-x. Effect of promoters on the catalytic performance of Ni/Al_2O_3 catalyst for partial oxidation of methane to syngas. React Kinet Catal Lett 2004;83:245–52.
[131] Chu Y, Li S, Lin J, Gu J, Yang Y. Partial oxidation of methane to carbon monoxide and hydrogen over NiO/La_2O_3/γ-Al_2O_3 catalyst. Appl Catal A: Gen 1996;134:67–80.
[132] Liu S, Xiong G, Yang W, Sheng S. The effect of Li and La on NiO/Al_2O_3 catalyst for CH_4/O_2 to syngas reaction. React Kinet Catal Lett 1999;68:243–7.
[133] González MG, Nichio NN, Moraweck B, Martin G. Role of chromium in the stability of Ni/Al_2O_3 catalysts for natural gas reforming. Mater Lett 2000;45:15–8.
[134] Wang W, Zhu H, Yang G, Park HJ, Jung DW, Kwak C, et al. A NiFeCu alloy anode catalyst for direct-methane solid oxide fuel cells. J Power Sources 2014;258:134–41.
[135] Dias JAC, Assaf JM. Autothermal reforming of methane over Ni/γ-Al_2O_3 catalysts: the enhancement effect of small quantities of noble metals. J Power Sources 2004;130:106–10.
[136] Choudhary VR, Prabhakar B, Rajput AM, Mamman AS. Oxidative conversion of methane to CO and H_2 over Pt or Pd containing alkaline and rare earth oxide catalysts. Fuel 1998;77:1477–81.
[137] Makarshin LL, Sadykov VA, Andreev DV, Gribovskii AG, Privezentsev VV, Parmon VN. Syngas production by partial oxidation of methane in a microchannel reactor over a Ni–Pt/$La_{0.2}Zr_{0.4}Ce_{0.4}O_x$ catalyst. Fuel Process Technol 2015;131:21–8.
[138] Vorontsov VA, Gribovskiy AG, Makarshin LL, Andreev DV, Ylianitsky VY, Parmon VN. Influence of a reaction mixture streamline on partial oxidation of methane in an asymmetric microchannel reactor. Int J Hydrog Energy 2014;39:325–30.
[139] Toscani LM, Zimicz MG, Casanova JR, Larrondo SA. Ni–Cu/$Ce_{0.9}Zr_{0.1}O_2$ bimetallic cermets for electrochemical and catalytic applications. Int J Hydrog Energy 2014;39:8759–66.
[140] Zhu Y, Zhang S, Shan J-j, Nguyen L, Zhan S, Gu X, et al. In situ surface chemistries and catalytic performances of ceria doped with palladium, platinum, and rhodium in methane partial oxidation for the production of syngas. ACS Catal 2013;3:2627–39.
[141] Basile F, Fornasari G, Trifirò F, Vaccari A. Partial oxidation of methane: effect of reaction parameters and catalyst composition on the thermal profile and heat distribution. Catal Today 2001;64:21–30.
[142] Benito P, Dal Santo V, De Grandi V, Marelli M, Fornasari G, Psaro R, et al. Coprecipitation versus chemical vapour deposition to prepare Rh/Ni bimetallic catalysts. Appl Catal B: Environ 2015;179:150–9.
[143] Sun W-Z, Jin G-Q, Guo X-Y. Partial oxidation of methane to syngas over Ni/SiC catalysts. Catal Commun 2005;6:135–9.
[144] Ding C, Ai G, Zhang K, Yuan Q, Han Y, Ma X, et al. Coking resistant Ni/ZrO_2@SiO_2 catalyst for the partial oxidation of methane to synthesis gas. Int J Hydrog Energy 2015;40:6835–43.
[145] Pal P, Singha RK, Saha A, Bal R, Panda AB. Defect-induced efficient partial oxidation of methane over nonstoichiometric Ni/CeO2 nanocrystals. J Phys Chem C 2015;119:13610–8.
[146] Chalupka KA, Jozwiak WK, Rynkowski J, Maniukiewicz W, Casale S, Dzwigaj S. Partial oxidation of methane on NixAlBEA and NixSiBEA zeolite catalysts: remarkable effect of preparation procedure and Ni content. Appl Catal B: Environ 2014;146:227–36.
[147] Pantaleo G, La Parola V, Deganello F, Calatozzo P, Bal R, Venezia AM. Synthesis and support composition effects on CH_4 partial oxidation over Ni–CeLa oxides.

Appl Catal B: Environ 2015;164:135–43.
[148] Yu C, Hu J, Zhou W, Fan Q. Novel Ni/CeO_2-Al_2O_3 composite catalysts synthesized by one-step citric acid complex and their performance in catalytic partial oxidation of methane. J Energy Chem 2014;23:235–43.
[149] Yan QG, Weng WZ, Wan HL, Toghiani H, Toghiani RK, Pittman Jr CU. Activation of methane to syngas over a Ni/TiO_2 catalyst. Appl Catal A: Gen 2003;239:43–58.
[150] Rui Z, Feng D, Chen H, Ji H. Anodic TiO_2 nanotube array supported nickel – noble metal bimetallic catalysts for activation of CH_4 and CO_2 to syngas. Int J Hydrog Energy 2014;39:16252–61.
[151] Ding C, Liu W, Wang J, Liu P, Zhang K, Gao X, et al. One step synthesis of mesoporous NiO–Al_2O_3 catalyst for partial oxidation of methane to syngas: the role of calcination temperature. Fuel 2015;162:148–54.
[152] Brackmann R, Perez CA, Schmal M. $LaCoO_3$ perovskite on ceramic monoliths – Pre and post reaction analyzes of the partial oxidation of methane. Int J Hydrog Energy 2014;39:13991–4007.
[153] Dedov AG, Loktev AS, Komissarenko DA, Mazo GN, Shlyakhtin OA, Parkhomenko KV, et al. Partial oxidation of methane to produce syngas over a neodymium–calcium cobaltate-based catalyst. Appl Catal A: Gen 2015;489:140–6.
[154] Staniforth J, Evans SE, Good OJ, Darton RJ, Ormerod RM. A novel perovskite based catalyst with high selectivity and activity for partial oxidation of methane for fuel cell applications. Dalton Trans 2014;43:15022–7.
[155] Yoon JS, Lim Y-S, Choi BH, Hwang HJ. Catalytic activity of perovskite-type doped $La_{0.08}Sr_{0.92}Ti_{1-x}M_xO_{3-\delta}$ (M = Mn, Fe, and Co) oxides for methane oxidation. Int J Hydrog Energy 2014;39:7955–62.
[156] Morales M, Espiell F, Segarra M. Performance and stability of $La_{0.5}Sr_{0.5}CoO_{3-\delta}$ perovskite as catalyst precursor for syngas production by partial oxidation of methane. Int J Hydrog Energy 2014;39:6454–61.
[157] Wang Y, Liao Q, Zhou L, Wang H. Oxygen permeability and structure stability of a novel cobalt-free perovskite $Gd_{0.33}Ba_{0.67}FeO_{3-\delta}$. J Membr Sci 2014;457:82–7.
[158] Li L, Yao Y, Sun B, Fei Z, Xia H, Zhao J, et al. Highly active and stable lanthanum-doped core–shell-structured Ni@SiO_2 catalysts for the partial oxidation of methane to syngas. ChemCatChem 2013;5:3781–7.
[159] Meng B, Zhang H, Qin J, Tan X, Ran R, Liu S. The catalytic effects of $La_{0.3}Sr_{0.7}Fe_{0.7}Cu_{0.2}Mo_{0.1}O_3$ perovskite and its hollow fibre membrane for air separation and methane conversion reactions. Sep Purif Technol 2015;147:406–13.
[160] Zhu DC, Xu XY, Feng SJ, Liu W, Chen CS. La2NiO4 tubular membrane reactor for conversion of methane to syngas. Catal Today 2003;82:151–6.
[161] Vernon PDF, Green MLH, Cheetham AK, Ashcroft AT. Partial oxidation of methane to synthesis gas, and carbon dioxide as an oxidising agent for methane conversion. Catal Today 1992;13:417–26.
[162] Abbasi R, Huang G, Istratescu GM, Wu L, Hayes RE. Methane oxidation over Pt, Pt: Pd, and Pd based catalysts: effects of pre-treatment. Can J Chem Eng 2015;93:1474–82.
[163] Santis-Alvarez AJ, Büchel R, Hild N, Stark WJ, Poulikakos D. Comparison of flame-made rhodium on Al_2O_3 or $Ce_{0.5}Zr_{0.5}O_2$ supports for the partial oxidation of methane. Appl Catal A: Gen 2014;469:275–83.
[164] Rostrup-Nielsen JR. Production of synthesis gas. Catal Today 1993;18:305–24.
[165] Kaydouh MN, El Hassan N, Davidson A, Casale S, El Zakhem H, Massiani P. Highly active and stable Ni/SBA-15 catalysts prepared by a "two solvents" method for dry reforming of methane. Microporous Mesoporous Mater 2016;220:99–109.
[166] Zhang J, Li F. Coke-resistant Ni@SiO_2 catalyst for dry reforming of methane. Appl Catal B: Environ 2015;176–177:513–21.
[167] Li Z, Mo L, Kathiraser Y, Kawi S. Yolk–satellite–shell structured Ni–Yolk@Ni@SiO_2 nanocomposite: superb catalyst toward methane CO_2 reforming reaction. ACS Catal 2014;4:1526–36.
[168] Son IH, Kwon S, Park JH, Lee SJ. High coke-resistance $MgAl_2O_4$ islands decorated catalyst with minimizing sintering in carbon dioxide reforming of methane. Nano Energy 2016;19:58–67.
[169] Odedairo T, Ma J, Chen J, Wang S, Zhu Z. Influences of doping Cr/Fe/Ta on the performance of Ni/CeO_2 catalyst under microwave irradiation in dry reforming of CH4. J Solid State Chem 2016;233:166–77.
[170] García-Diéguez M, Pieta IS, Herrera MC, Larrubia MA, Alemany LJ. Improved Pt-Ni nanocatalysts for dry reforming of methane. Appl Catal A: Gen 2010;377:191–9.
[171] Makri MM, Vasiliades MA, Petallidou KC, Efstathiou AM. Effect of support composition on the origin and reactivity of carbon formed during dry reforming of methane over 5 wt% Ni/$Ce_{1-x}M_xO_{2-\delta}$ (M = Zr^{4+}, Pr^{3+}) catalysts. Catal Today 2016;259, Part 1:150–64.
[172] Wang F, Xu L, Zhang J, Zhao Y, Li H, Li HX, et al. Tuning the metal-support interaction in catalysts for highly efficient methane dry reforming reaction. Appl Catal B: Environ 2016;180:511–20.
[173] Kim SS, Lee SM, Won JM, Yang HJ, Hong SC. Effect of Ce/Ti ratio on the catalytic activity and stability of Ni/CeO_2–TiO_2 catalyst for dry reforming of methane. Chem Eng J 2015;280:433–40.
[174] Fang X, Peng C, Peng H, Liu W, Xu X, Wang X, et al. Methane dry reforming over coke-resistant mesoporous Ni-Al_2O_3 catalysts prepared by evaporation-induced self-assembly method. ChemCatChem 2015;7:3753–62.
[175] Zhang S, Shi C, Chen B, Zhang Y, Zhu Y, Qiu J, et al. Catalytic role of β-M_o2C in DRM catalysts that contain Ni and Mo. Catal Today 2015;258, Part 2:676–83.
[176] Das S, Thakur S, Bag A, Gupta MS, Mondal P, Bordoloi A. Support interaction of Ni nanocluster based catalysts applied in CO_2 reforming. J Catal 2015;330:46–60.
[177] Zhang S, Shi C, Chen B, Zhang Y, Qiu J. An active and coke-resistant dry reforming catalyst comprising nickel–tungsten alloy nanoparticles. Catal Commun 2015;69:123–8.
[178] Paksoy AI, Caglayan BS, Aksoylu AE. A study on characterization and methane dry reforming performance of Co–Ce/ZrO_2 catalyst. Appl Catal B: Environ 2015;168–169:164–74.
[179] Ayodele BV, Khan MR, Cheng CK. Catalytic performance of ceria-supported cobalt catalyst for CO-rich hydrogen production from dry reforming of methane. Int J Hydrog Energy 2016;41:198–207.
[180] Zhu Y, Zhang S, Chen B, Zhang Z, Shi C. Effect of Mg/Al ratio of NiMgAl mixed oxide catalyst derived from hydrotalcite for carbon dioxide reforming of methane. Catal Today.
[181] Li L, Zhou L, Ould-Chikh S, Anjum DH, Kanoun MB, Scaranto J, et al. Controlled surface segregation leads to efficient coke-resistant nickel/platinum bimetallic catalysts for the dry reforming of methane. ChemCatChem 2015;7:819–29.
[182] Zhang G, Hao L, Jia Y, du Y, Zhang Y. CO_2 reforming of CH_4 over efficient bimetallic Co–Zr/AC catalyst for H_2 production. Int J Hydrog Energy 2015;40:12868–79.
[183] Tankov I, Arishtirova K, Bueno JMC, Damyanova S. Surface and structural features of Pt/PrO_2–Al_2O_3 catalysts for dry methane reforming. Appl Catal A: Gen 2014;474:135–48.
[184] Múnera J, Faroldi B, Frutis E, Lombardo E, Cornaglia L, Carrazán SG. Supported Rh nanoparticles on CaO–SiO_2 binary systems for the reforming of methane by carbon dioxide in membrane reactors. Appl Catal A: Gen 2014;474:114–24.
[185] Wu H, Pantaleo G, La Parola V, Venezia AM, Collard X, Aprile C, et al. Bi- and trimetallic Ni catalysts over Al_2O_3 and Al_2O_3-MO_x (M = Ce or Mg) oxides for methane dry reforming: Au and Pt additive effects. Appl Catal B: Environ 2014;156–157:350–61.
[186] Chen W, Zhao G, Xue Q, Chen L, Lu Y. High carbon-resistance Ni/$CeAlO_3$-Al_2O_3 catalyst for CH_4/CO_2 reforming. Appl Catal B: Environ 2013;136–137:260–8.
[187] Asencios YJO, Assaf EM. Combination of dry reforming and partial oxidation of methane on NiO–MgO–ZrO_2 catalyst: effect of nickel content. Fuel Process Technol 2013;106:247–52.
[188] Valderrama G, Urbina de Navarro C, Goldwasser MR. CO_2 reforming of CH_4 over Co–La-based perovskite-type catalyst precursors. J Power Sources 2013;234:31–7.
[189] Arandiyan H, Li J, Ma L, Hashemnejad SM, Mirzaei MZ, Chen J, et al. Methane reforming to syngas over $LaNixFe_{1-x}O_3$ ($0 \le x \le 1$) mixed-oxide perovskites in the presence of CO_2 and O_2. J Ind Eng Chem 2012;18:2103–14.
[190] Tao K, Zhou S, Zhang Q, Kong C, Ma Q, Tsubaki N, et al. Sol-gel auto-combustion synthesis of Ni-$Ce_xZr_{1-x}O_2$ catalysts for carbon dioxide reforming of methane. RSC Adv 2013;3:22285–94.
[191] Moradi GR, Rahmanzadeh M. The influence of partial substitution of alkaline earth with La in the $LaNiO_3$ perovskite catalyst. Catal Commun 2012;26:169–72.
[192] Djinović P, Batista J, Pintar A. Efficient catalytic abatement of greenhouse gases: methane reforming with CO_2 using a novel and thermally stable Rh–CeO_2 catalyst. Int J Hydrog Energy 2012;37:2699–707.
[193] García-Diéguez M, Herrera MC, Pieta IS, Larrubia MA, Alemany LJ. NiBa catalysts for CO_2-reforming of methane. Catal Commun 2010;11:1133–6.
[194] Chen J, Yao C, Zhao Y, Jia P. Synthesis gas production from dry reforming of methane over $Ce_{0.75}Zr_{0.25}O_2$-supported Ru catalysts. Int J Hydrog Energy 2010;35:1630–42.
[195] Wu JCS, Chou H-C. Bimetallic Rh–Ni/BN catalyst for methane reforming with CO_2. Chem Eng J 2009;148:539–45.
[196] Khalesi A, Arandiyan HR, Parvari M. Production of syngas by CO_2 reforming on $M_xLa_{1-x}Ni_{0.3}Al_{0.7}O_{3-\delta}$ (M = Li, Na, K) catalysts. Ind Eng Chem Res 2008;47:5892–8.
[197] Lima SM, Assaf JM, Peña MA, Fierro JLG. Structural features of $La_{1-x}Ce_xNiO_3$ mixed oxides and performance for the dry reforming of methane. Appl Catal A: Gen 2006;311:94–104.
[198] Gallego GS, Batiot-Dupeyrat C, Barrault J, Florez E, Mondragón F. Dry reforming of methane over $LaNi_{1-y}B_yO_{3\pm\delta}$ (B = Mg, Co) perovskites used as catalyst precursor. Appl Catal A: Gen 2008;334:251–8.
[199] GCd Araujo, SMd Lima, Assaf, Peña JM, Fierro MA, do JLG, et al. M. Catalytic evaluation of perovskite-type oxide $LaNi_{1-x}Ru_xO_3$ in methane dry reforming. Catal Today 2008;133–135:129–35.
[200] Horváth A, Stefler G, Geszti O, Kienneman A, Pietraszek A, Guczi L. Methane dry reforming with CO_2 on CeZr-oxide supported Ni, NiRh and NiCo catalysts prepared by sol–gel technique: relationship between activity and coke formation. Catal Today 2011;169:102–11.
[201] Rivas ME, Fierro JLG, Goldwasser MR, Pietri E, Pérez-Zurita MJ, Griboval-Constant A, et al. Structural features and performance of $LaNi_{1-x}Rh_xO_3$ system for the dry reforming of methane. Appl Catal A: Gen 2008;344:10–9.
[202] García-Diéguez M, Pieta IS, Herrera MC, Larrubia MA, Alemany LJ. Nanostructured Pt- and Ni-based catalysts for CO_2-reforming of methane. J Catal 2010;270:136–45.
[203] Hou Z, Yashima T. Small amounts of Rh-promoted Ni catalysts for methane reforming with CO_2. Catal Lett 2003;89:193–7.
[204] Xi H, Hou X, Liu Y, Qing S, Gao Z. Cu–Al spinel oxide as an efficient catalyst for methanol steam reforming. Angew Chem Int Ed 2014;53:11886–9.
[205] Iulianelli A, Ribeirinha P, Mendes A, Basile A. Methanol steam reforming for hydrogen generation via conventional and membrane reactors: a review. Renew Sustain Energy Rev 2014;29:355–68.
[206] Zanchet D, Santos JBO, Damyanova S, Gallo JMR, Bueno C, Toward JM. Understanding metal-catalyzed ethanol reforming. ACS Catal 2015;5:3841–63.
[207] Yong ST, Ooi CW, Chai SP, Wu XS. Review of methanol reforming-Cu-based catalysts, surface reaction mechanisms, and reaction schemes. Int J Hydrog Energy 2013;38:9541–52.
[208] Lytkina AA, Zhilyaeva NA, Ermilova MM, Orekhova NV, Yaroslavtsev AB. Influence of the support structure and composition of Ni–Cu-based catalysts on hydrogen production by methanol steam reforming. Int J Hydrog Energy 2015;40:9677–84.

[209] Ma Y, Guan G, Phanthong P, Hao X, Huang W, Tsutsumi A, et al. Catalytic activity and stability of nickel-modified molybdenum carbide catalysts for steam reforming of methanol. J Phys Chem C 2014;118:9485–96.

[210] Kuc J, Matam SK, Neumann M, Yoon S, Thiel P, Armbrüster M, et al. Methanol steam reforming on $LaCo_{1-x-y}Pd_xZn_yO_{3\pm\delta}$. Catal Today.

[211] Hou T, Yu B, Zhang S, Xu T, Wang D, Cai W. Hydrogen production from ethanol steam reforming over Rh/CeO_2 catalyst. Catal Commun 2015;58:137–40.

[212] Ferencz Z, Erdőhelyi A, Baán K, Oszkó A, Óvári L, Kónya Z, et al. Effects of support and Rh additive on co-based catalysts in the ethanol steam reforming reaction. ACS Catal 2014;4:1205–18.

[213] González-Gil R, Chamorro-Burgos I, Herrera C, Larrubia MA, Laborde M, Mariño F, et al. Production of hydrogen by catalytic steam reforming of oxygenated model compounds on Ni-modified supported catalysts. Simulation and experimental study. Int J Hydrog Energy.

[214] Garbarino G, Wang C, Valsamakis I, Chitsazan S, Riani P, Finocchio E, et al. A study of Ni/Al_2O_3 and Ni–La/Al_2O_3 catalysts for the steam reforming of ethanol and phenol. Appl Catal B: Environ 2015;174–175:21–34.

[215] Osorio-Vargas P, Campos CH, Navarro RM, Fierro JLG, Reyes P. Rh/Al_2O_3–La_2O_3 catalysts promoted with CeO_2 for ethanol steam reforming reaction. J Mol Catal A: Chem 2015;407:169–81.

[216] Zeng G, Liu Q, Gu R, Zhang L, Li Y. Synergy effect of MgO and ZnO in a Ni/Mg–Zn–Al catalyst during ethanol steam reforming for H2-rich gas production. Catal Today 2011;178:206–13.

[217] Aceves Olivas DY, Baray Guerrero MR, Escobedo Bretado MA, Marques da Silva Paula M, Salinas Gutiérrez J, Guzmán Velderrain V, et al. Enhanced ethanol steam reforming by CO_2 absorption using CaO, CaO*MgO or Na_2ZrO_3. Int J Hydrog Energy 2014;39:16595–607.

[218] Sun J, Karim AM, Mei D, Engelhard M, Bao X, Wang Y. New insights into reaction mechanisms of ethanol steam reforming on Co–ZrO_2. Appl Catal B: Environ 2015;162:141–8.

[219] Dancini-Pontes I, DeSouza M, Silva FA, Scaliante MHNO, Alonso CG, Bianchi GS, et al. Influence of the CeO_2 and Nb_2O_5 supports and the inert gas in ethanol steam reforming for H_2 production. Chem Eng J 2015;273:66–74.

[220] Valle B, Aramburu B, Remiro A, Bilbao J, Gayubo AG. Effect of calcination/reduction conditions of Ni/La_2O_3–αAl_2O_3 catalyst on its activity and stability for hydrogen production by steam reforming of raw bio-oil/ethanol. Appl Catal B: Environ 2014;147:402–10.

[221] Morales M, Segarra M. Steam reforming and oxidative steam reforming of ethanol over $La_{0.6}Sr_{0.4}CoO_{3-\delta}$ perovskite as catalyst precursor for hydrogen production. Appl Catal A: Gen 2015;502:305–11.

[222] Wang W, Chen Y, Wang F, Tade MO, Shao Z. Enhanced electrochemical performance, water storage capability and coking resistance of a Ni + $BaZr_{0.1}Ce_{0.7}Y_{0.1}Yb_{0.1}O_{3-\delta}$ anode for solid oxide fuel cells operating on ethanol. Chem Eng Sci 2015;126:22–31.

[223] Chen L-C, Cheng H, Chiang C-W, Lin SD. Sustainable hydrogen production by ethanol steam reforming using a partially reduced copper–nickel oxide catalyst. ChemSusChem 2015;8:1787–93.

[224] Kim D, Kwak BS, Park N-K, Han GB, Kang M. Dynamic hydrogen production from ethanol steam-reforming reaction on Ni_xMo_y/SBA-15 catalytic system. Int J Energy Res 2015;39:279–92.

[225] Dan M, Mihet M, Tasnadi-Asztalos Z, Imre-Lucaci A, Katona G, Lazar MD. Hydrogen production by ethanol steam reforming on nickel catalysts: effect of support modification by CeO_2 and La_2O_3. Fuel 2015;147:260–8.

[226] Wang W, Su C, Ran R, Zhao B, Shao ZO, Tade M, et al. Nickel-based anode with water storage capability to mitigate carbon deposition for direct ethanol solid oxide fuel cells. ChemSusChem 2014;7:1719–28.

[227] Shishido T, Yamamoto Y, Morioka H, Takaki K, Takehira K. Active Cu/ZnO and Cu/ZnO/Al_2O_3 catalysts prepared by homogeneous precipitation method in steam reforming of methanol. Appl Catal A: Gen 2004;263:249–53.

[228] Jones SD, Hagelin-Weaver HE. Steam reforming of methanol over CeO_2- and ZrO_2-promoted Cu-ZnO catalysts supported on nanoparticle Al_2O_3. Appl Catal B: Environ 2009;90:195–204.

[229] Liu Q, Wang L-C, Chen M, Liu Y-M, Cao Y, He H-Y, et al. Waste-free soft reactive grinding synthesis of high-surface-area copper–manganese spinel oxide catalysts highly effective for methanol steam reforming. Catal Lett 2008;121:144–50.

[230] Wang L-C, Liu Y-M, Chen M, Cao Y, He H-Y, Wu G-S, et al. Production of hydrogen by steam reforming of methanol over Cu/ZnO catalysts prepared via a practical soft reactive grinding route based on dry oxalate-precursor synthesis. J Catal 2007;246:193–204.

[231] Jeong H, Kim KI, Kim TH, Ko CH, Park HC, Song IK. Hydrogen production by steam reforming of methanol in a micro-channel reactor coated with Cu/ZnO/ZrO_2/Al_2O_3 catalyst. J Power Sources 2006;159:1296–9.

[232] Matsumura Y, Ishibe H. Suppression of CO by-production in steam reforming of methanol by addition of zinc oxide to silica-supported copper catalyst. J Catal 2009;268:282–9.

[233] Huang G, Liaw B-J, Jhang C-J, Chen Y-Z. Steam reforming of methanol over CuO/ZnO/CeO_2/ZrO_2/Al_2O_3 catalysts. Appl Catal A: Gen 2009;358:7–12.

[234] Agrell J, Birgersson H, Boutonnet M, Melián-Cabrera I, Navarro RM, Fierro JLG. Production of hydrogen from methanol over Cu/ZnO catalysts promoted by ZrO_2 and Al_2O_3. J Catal 2003;219:389–403.

[235] Patel S, Pant KK. Activity and stability enhancement of copper–alumina catalysts using cerium and zinc promoters for the selective production of hydrogen via steam reforming of methanol. J Power Sources 2006;159:139–43.

[236] Liu Y, Hayakawa T, Tsunoda T, Suzuki K, Hamakawa S, Murata K, et al. Steam reforming of methanol over Cu/CeO_2 catalysts studied in comparison with Cu/ZnO and Cu/Zn(Al)O catalysts. Top Catal 2003;22:205–13.

[237] Papavasiliou J, Avgouropoulos G, Ioannides T. Steam reforming of methanol over copper–manganese spinel oxide catalysts. Catal Commun 2005;6:497–501.

[238] Biswas P, Kunzru D. Steam reforming of ethanol on Ni–CeO_2–ZrO_2 catalysts: effect of doping with copper, cobalt and calcium. Catal Lett 2007;118:36–49.

[239] Augusto BL, Noronha FB, Fonseca FC, Tabuti FN, Colman RC, Mattos LV. Nickel/gadolinium-doped ceria anode for direct ethanol solid oxide fuel cell. Int J Hydrog Energy 2014;39:11196–209.

[240] Rossetti I, Lasso J, Finocchio E, Ramis G, Nichele V, Signoretto M, et al. TiO_2-supported catalysts for the steam reforming of ethanol. Appl Catal A: Gen 2014;477:42–53.

[241] Chen L-C, Lin SD. Effects of the pretreatment of CuNi/SiO_2 on ethanol steam reforming: influence of bimetal morphology. Appl Catal B: Environ 2014;148–149:509–19.

[242] Moraes TS, Neto RCR, Ribeiro MC, Mattos LV, Kourtelesis M, Ladas S, et al. The study of the performance of PtNi/Ce_O2–nanocube catalysts for low temperature steam reforming of ethanol. Catal Today 2015;242, Part A:35–49.

[243] Chiou JYZ, Lee C-L, Ho K-F, Huang H-H, Yu S-W, Wang C-B. Catalytic performance of Pt-promoted cobalt-based catalysts for the steam reforming of ethanol. Int J Hydrog Energy 2014;39:5653–62.

[244] Fang W, Paul S, Capron M, Biradar AV, Umbarkar SB, Dongare MK, et al. Highly loaded well dispersed stable Ni species in $Ni_xMg_2AlO_Y$ nanocomposites: application to hydrogen production from bioethanol. Appl Catal B: Environ 2015;166–167:485–96.

[245] Kwak BS, Lee G, Park S-M, Kang M. Effect of MnO_x in the catalytic stabilization of Co_2MnO_4 spinel during the ethanol steam reforming reaction. Appl Catal A: Gen 2015;503:165–75.

[246] Greluk M, Rybak P, Słowik G, Rotko M, Machocki A. Comparative study on steam and oxidative steam reforming of ethanol over 2KCo/Zr_O2 catalyst. Catal Today 2015;242, Part A:50–9.

[247] Chen SQ, Li YD, Liu Y, Bai X. Regenerable and durable catalyst for hydrogen production from ethanol steam reforming. Int J Hydrog Energy 2011;36:5849–56.

[248] Zhao L, Wei Y, Huang Y, Liu Y. $La_{1-x}K_xFe_{0.7}Ni_{0.3}O_3$ catalyst for ethanol steam reforming—the effect of K-doping. Catal Today.

[249] Liu F, Qu Y, Yue Y, Liu G, Liu Y. Nano bimetallic alloy of Ni-Co obtained from $LaCo_xNi_{1-x}O_3$ and its catalytic performance for steam reforming of ethanol. RSC Adv 2015;5:16837–46.

[250] Wang Z, Wang C, Chen S, Liu Y. Co–Ni bimetal catalyst supported on perovskite-type oxide for steam reforming of ethanol to produce hydrogen. Int J Hydrog Energy 2014;39:5644–52.

[251] Lee G, Kim D, Kwak BS, Kang M. Hydrogen rich production by ethanol steam reforming reaction over Mn/$Co_{10}Si_{90}$MCM-48 catalysts. Catal Today 2014;232:139–50.

[252] Zou J, Yu B, Zhang S, Zhang J, Chen Y, Cui L, et al. Hydrogen production from ethanol over Ir/CeO_2 catalyst: effect of the calcination temperature. Fuel 2015;159:741–50.

[253] Chiou JYZ, Siang J-Y, Yang S-Y, Ho K-F, Lee C-L, Yeh C-T, et al. Pathways of ethanol steam reforming over ceria-supported catalysts. Int J Hydrog Energy 2012;37:13667–73.

[254] Wang F, Cai W, Provendier H, Schuurman Y, Descorme C, Mirodatos C, et al. Hydrogen production from ethanol steam reforming over Ir/CeO2 catalysts: enhanced stability by PrO_x promotion. Int J Hydrog Energy 2011;36:13566–74.

[255] Frusteri F, Freni S, Spadaro L, Chiodo V, Bonura G, Donato S, et al. H_2 production for MC fuel cell by steam reforming of ethanol over MgO supported Pd, Rh, Ni and Co catalysts. Catal Commun 2004;5:611–5.

[256] He Z, Yang M, Wang X, Zhao Z, Duan A. Effect of the transition metal oxide supports on hydrogen production from bio-ethanol reforming. Catal Today 2012;194:2–8.

[257] de Lima SM, Silva AM, Graham UM, Jacobs G, Davis BH, Mattos LV, et al. Ethanol decomposition and steam reforming of ethanol over $CeZrO_2$ and Pt/$CeZrO_2$ catalyst: reaction mechanism and deactivation. Appl Catal A: Gen 2009;352:95–113.

[258] Argyle MD, Bartholomew CH. Heterogeneous catalyst deactivation and regeneration: a review. Catalysts 2015;5:145–269.

[259] Ocsachoque MA, Russman JIE, Irigoyen B, Gazzoli D, Gonzalez MG. Experimental and theoretical study about sulfur deactivation of Ni/CeO_2 and Rh/CeO_2 catalysts. Mater Chem Phys 2016;172:69–76.

[260] Zhou L, Li L, Wei N, Li J, Basset J-M. Effect of $NiAl_2O_4$ formation on Ni/Al_2O_3 stability during dry reforming of methane. ChemCatChem 2015;7:2508–16.

[261] Hu Y, Wang X, Tan M, Zou X, Ding W, Lu X. Perovskite $LaNiO_3$ nanocrystals inside SBA-15 silica: high stability and anti-coking performance in the pre-reforming of liquefied petroleum gas at a low steam-to-carbon molar ratio. ChemCatChem 2016;8:1055–8.

[262] Hanna J, Lee WY, Shi Y, Ghoniem AF. Fundamentals of electro- and thermochemistry in the anode of solid-oxide fuel cells with hydrocarbon and syngas fuels. Prog Energy Combust Sci 2014;40:74–111.

[263] Putna ES, Stubenrauch J, Vohs JM, Gorte RJ. Ceria-based anodes for the direct oxidation of methane in solid oxide fuel cells. Langmuir 1995;11:4832–7.

[264] Murray EP, Tsai T, Barnett S. A direct-methane fuel cell with a ceria-based anode. Nature 1999;400:649–51.

[265] Park SD, Vohs JM, Gorte RJ. Direct oxidation of hydrocarbons in a solid-oxide fuel cell. Nature 2000;404:265–7.

[266] Kee RJ, Zhu H, Sukeshini AM, Jackson GS. Solid oxide fuel cells: operating principles, current challenges, and the role of syngas. Combust Sci Technol 2008;180:1207–44.

[267] Cowin PI, Petit CT, Lan R, Irvine JT, Tao SW. Recent progress in the development of anode materials for solid oxide fuel cells. Adv Energy Mater 2011;1:314–32.

[268] Kwon BW, Ellefson C, Breit J, Kim J, Norton MG, Ha S. Molybdenum dioxide-based

anode for solid oxide fuel cell applications. J Power Sources 2013;243:203–10.
[269] Jeong J, Baek S-W, Bae J. A diesel-driven, metal-based solid oxide fuel cell. J Power Sources 2014;250:98–104.
[270] Kwon BW, Hu S, Marin-Flores O, Norton MG, Kim J, Scudiero L, et al. High-performance molybdenum dioxide-based anode for dodecane-fueled solid-oxide fuel cells (SOFCs). Energy Technol 2014;2:425–30.
[271] Lin J, Trabold TA, Walluk MR, Smith DF. Bio-fuel reformation for solid oxide fuel cell applications. Part 3: biodiesel-diesel blends. Int J Hydrog Energy 2014;39:196–208.
[272] McIntosh S, He HP, Lee SI, Costa-Nunes O, Krishnan VV, Vohs JM, et al. An examination of carbonaceous deposits in direct-utilization SOFC anodes. J Electrochem Soc 2004;151:A604–8.
[273] Ruiz-Morales JC, Canales-Vazquez J, Savaniu C, Marrero-Lopez D, Zhou WZ, Irvine JTS. Disruption of extended defects in solid oxide fuel cell anodes for methane oxidation. Nature 2006;439:568–71.
[274] Petit CT, Lan R, Cowin PI, Irvine JT, Tao S. Structure, conductivity and redox reversibility of Ca-doped cerium metavanadate. J Mater Chem 2011;21:8854–61.
[275] Huang YH, Dass RI, Xing ZL, Goodenough JB. Double perovskites as anode materials for solid-oxide fuel cells. Science 2006;312:254–7.
[276] Chen Y, Zhang Y, Lin Y, Yang Z, Su D, Han M, et al. Direct-methane solid oxide fuel cells with hierarchically porous Ni-based anode deposited with nanocatalyst layer. Nano Energy 2014;10:1–9.